[47] I. R. Johnson and S. K. Barton, “Signal Processing Hardware in a Radio LAN Demonstrator”, Wireless Personal Communications special issue on HIPERLAN, Vol. 3, No. 4, 1996, pp 429 - 443.

[48] P. F. M. Smulders, “Error Control in ATM-Based Indoor Radio LANs”, IEEE 5th Int. Symp. on Personal, Indoor and Mobile Radio Comm., The Hague, Sept. 1994, pp. 237-241.

[49] P. Matuszczak, W. Holubowicz, and M. Moeneclaey, “Satellite Modems Using Multiplexed and Concatenated Codes”, 3rd International Symposium on Communication Theory and Applications, Ambleside 1995, pp. 347-354.

[50] P. F. M. Smulders and C. Blondia, “Application of the Asynchronous Transfer Mode in Indoor Radio Networks”, WCN’94, The Hague, pp. 839-843, Sept. 1994.

[51] P. F. M. Smulders, “Error Control in ATM-Based Indoor Radio LANs”, Proc. of the IEEE 5th Int. Symp. on Personal, Indoor and Mobile Radio Comm., The Hague, pp. 237-241, Sept. 1994.

[52] R. Prasad, “Performance analysis of mobile packet radio networks in real channels with inhibit sense multiple access”, IEE Proc-I, Vol 138, No.5, October 1991.

[53] R. Prasad and C. Y. Liu, “Throughput analysis of some mobile packet radio protocols in Rician fading channels”, IEE Proc-I, Vol 139, No.3, June 1992.

[54] K. Fu, Y. J. Guo and S. K. Barton, “Performance of the EY-NPMA Protocol with Hidden Nodes”, Wireless Personal Communications special issue on HIPERLAN, Vol. 4, No. 1, 1997, pp 41 - 50.

Dispersive Channel", Electronics Letters Vol. 29, No. 24, 25th November 1993, pp. 2048-2085.

[37] T. A. H. Wilkinson, T. G. C. Phipps and S. K. Barton, "A report on HIPERLAN Standardisation", International Journal on Wireless Information Networks, Vol 2, No 2, 1995, pp. 99-119.

[38] L. Vandendorpe and O. van de Wiel, "Performance Analysis of Linear MIMO Equalisers for Multitone DS/SS Systems in Multipath Channels", Wireless Personal Communications, Special Issue on Multicarrier Techniques, Vol. 2, No 1-2, 1995, pp. 145-165.

[39] G. J. M. Janssen, L. Maranatha, and R. Prasad, "Evaluation of BER Performance for Measured Indoor Microwave Channels Using Quasi-Coherent Combining of Multiple Antenna Signals", pp.239-253 in Mobile and Personal Communications, Proc. 2nd Joint COST 227/231 Workshop, Firenze, 20-21 April 1995, ed. E del Re, Elsevier, Amsterdam, 1995.

[40] G. J. M. Janssen, "Dual-Signal Receiver Structures for Simultaneous Reception of Two BPSK Modulated Co-Channel Signals Using Signal Cancellation", Wireless Personal Communications, vol. 1, no. 1, 1994, pp. 43-59.

[41] P. F. M. Smulders and H. T. Müskens, "Performance of Decision Feedback Equalisation in mm-Wave Indoor Radio Systems", IEEE 2nd Int. Symp. on Univ. Personal Commun., Ottawa, Oct. 1993, pp. 890-893.

[42] M. Li, A. Nix, J. Marvill, M. A. Beach, T. A. H. Wilkinson, I. R. Johnson, and S.K. Barton, "Radio LANs Air Interface Technique Using Equalisation", WCN'94, The Hague, 21-23rd September 1994, pp. 964-968.

[43] C. Tellambura, Y. J. Guo, and S. K. Barton, "Equaliser Performance for HIPERLAN in Indoor Channels", Wireless Personal Communications special issue on HIPERLAN, Vol. 3, No. 4, 1996, pp 397 - 410.

[44] C. Tellambura, Y. J. Guo, and S. K. Barton, "Co-channel and Self Interference Analysis for Indoor Wireless Channels", Wireless Personal Communications special issue on HIPERLAN, Vol. 3, No. 4, 1996, pp 411 - 419.

[45] I. R. Johnson, T. A. H. Wilkinson, A. E. Jones, S. K. Barton, M. Li, A. Nix, J. Marvill, and M. A. Beach, "On Suitable Codes for Frame Synchronisation in Packet Radio LANs", 44th Vehicular Technology Conference, Stockholm, 7-11th June 1994, pp. 1421-1424.

[46] D. A. G. Gillies, Y. J. Guo, and S. K. Barton, "Synchronisation Techniques for HIPERLAN", Wireless Personal Communications special issue on HIPERLAN, Vol. 4, No. 1, 1997, pp 1 - 10.

[24] N. D. Hawkins, R. Steele, D.C. Rickard and C.R. Shepherd, "Path Loss Characteristics of 60 GHz Transmissions", Electron. Lett., Vol. 21, No. 22, pp. 1054-1055, 24th Oct. 1985.

[25] L. M. Correia and P. O. Francês, "A Propagation Model for the Estimation of the Average Power in an Outdoor Environment in the millimetre waveband", IEEE 44th Vehicular Technology Conference, Stockholm, Sweden, June 1994.

[26] ITU-R Rep. 719-2, Recommendations and Reports of the CCIR, Vol. V, ITU, Geneva, 1986.

[27] ITU-R Rep. 721-2, Recommendations and Reports of the CCIR, Vol. V, ITU, Geneva, 1986.

[28] G. Løvnes, S. E. Paulsen and R. H. Rækken, "A Versatile Channel Sounder for Millimetre Wave Measurements", 4th IEEE International Symposium on Personal, Indoor and Mobile Radio Communications, Yokohama, Japan, Sep. 8-11, 1993

[29] G. Løvnes, J. J. Reis and R. H. Rækken, "Channel Sounding Measurements at 59 GHz in City Streets", 5th IEEE International Symposium on Personal, Indoor and Mobile Radio Communications, The Hague, The Netherlands, Sep. 21-23, 1994.

[30] E. Antonsen, G. Løvnes, J. J. Reis and R. H. Rækken, "59 GHz Wideband Propagation Measurements", Telenor R&D Report TF R 36/94, Kjeller, Norway, 1994.

[31] J. J. Reis and L. M. Correia, "A Propagation Model for Outdoor Mobile Communications at the Millimetre Waveband in Urban Scenarios", COST231 TD(95)002, Bern, Jan. 1995.

[32] H. Aghvami, I. D. Robertson, and S. A. Mohamed, "High Bit-Rate Indoor Radio Communications", 3rd IEE Conference on Telecommunications, March 1991, pp. 101-106.

[33] H. Amca and P. A. Watson, "Simulation of MPSK and Wideband FM in Multipath LOS Channels Subject to Co-Channel Interference", COST231 TD (92) 109, Helsinki, Sep. 1992.

[34] P. F. M. Smulders and H. T. Müskens, "Bit Rate Performance of Millimetre-Wave Indoor Radio Systems", Electron. Lett., Vol. 28, No 23, Nov. 1992, pp. 2152-2153.

[35] T. A. Wilkinson and S. K. Barton, "Spread Spectrum for Radio Local Area Networks", URSI International Symposium on Signals, Systems and Electronics, Paris, 1-4 September 1992, pp. 60-63.

[36] T. A. H. Wilkinson, I. R. Johnson, and S. K. Barton, "Performance of Direct Sequence Spread Spectrum ISM-Band Radio LANs in a Multipath Time

[10] G. Dahlquist and A. Björck, “Numerical Methods”, Prentice-Hall, Englewood Clifs, N.J., 1974

[11] K. Sato, T. Manabe, I. Ihara, Y. Kasashima, and K. Yamaki, “Measurement of Reflectivities of Interior Construction Materials at 60 GHz” (in Japanese), Tech. Report of IEICE Japan, AP 93-36, June 1993

[12] J. Lähteenmäki, “Modelling of the Indoor Short Range Propagation Channel”, 24th European Microwave Conference, Workshop on short range radio communications, Cannes, Sep. 1994, pp 167 - 172.

[13] S. Guérin, “Indoor Wideband and Narrowband Propagation Measurements around 60.5 GHz in Empty and Furnished Room”, VTC’96, April 28 - May 1, Atlanta, GA.

[14] L. M. Correia and P. O. Francês, “Transmission and Isolation of Signals in Buildings at 60 GHz”, International Symposium on Personal, Indoor and Mobile Radio Communications, Toronto, Sep. 27-29, 1995.

[15] P. F. M. Smulders, A. G. Wagemans, “Wideband measurements of mm-wave indoor radio channels”, Proc. of the IEEE 3th Int. Symp. on Personal, Indoor and Mobile Radio Commun, Oct 1992., pp. 329-333.

[16] P. F. M. Smulders, “Broadband Wireless LANs: A Feasibility Study”, Ph.D. thesis, ISBN: 90-386-0100-X, 1995.

[17] G. Kadel, "Doppler analysis of wide-band propagation measurements", Nachrichtentechnik & Elektronik, Berlin 42 (1662), pp 13 (in German).

[18] P. F. M. Smulders, A.G. Wagemans, “Biconical Horn Antennas for Uniform Coverage in Indoor Areas at Mm-Wave Frequencies”, IEEE Trans. Veh. Technol., Vol. VT-43, no. 4, pp. 897-901, Nov. 1994.

[19] P. F. M. Smulders, “Geometrical optics model for millimetre-wave indoor radio propagation”, Electr. Lett., Vol. 29, pp. 1174-1176, June 1993.

[20] P. A. Watson, “Modelling radio propagation at millimetre wavelengths for communications and remote sensing”, 7th International Conference on Antennas and Propagation, Apr. 1991.

[21] K. Gunmar, “Broadband Technique for Car to Car Communication at 60 GHz”, COST 231 TD(91)041, Lund, Sweden, June 1991.

[22] Z. Ghebretensaé, “Simulation of Beacon-Vehicle Communications for Drive Applications”, COST 231 TD(92)053, Leeds, U.K., Apr. 1992.

[23] A. R. Tharek and J. P. McGeehan, “Outdoor Propagation Measurements in the Millimetre Wave Band at 60 GHz”, Military Microwaves'88, July 1988.

HIPERLAN application are also considered. The section also includes material on synchronisation in HIPERLAN and channel coding for wideband radio systems.

In section 8.6 MAC protocols for ATM access to the public B-ISDN, for random access to a wired backbone network, and for ad-hoc networks are described. The first uses a request/permit mechanism to control the access to the shared medium. The available capacity is allocated by means of a global FIFO queue in so that the peak bit rate is enforced. In the second, the uplink is declared busy or free by inhibit bits transmitted on the downlink. This enables RSs to avoid collisions. In the ad-hoc networks there is no BS to control access to the channel so a distributed protocol must be used. Two contention resolution protocols based on sensing the channel at the transmitter and one based on a handshake procedure are described.

8.8 References

[1] J. J. G. Fernandes, P. A. Watson and J. C. Neves, “Wireless LANs: Physical Properties of Infrared Systems vs Mmw Systems”, IEEE Communications Magazine, August, 1994

[2] P. F. M. Smulders, “Feasibility Considerations of Broadband Indoor Networks”, Proc. of the Int. Symp. on Subscriber Loops and Services '91, April 1991, pp. 76-80.

[3] P. Blakeborough, “Reflection Coefficients in the Range 8 to 50 GHz for Typical Indoor Building Materials”, COST 231 TD(92)050, Leeds, Apr. 1992

[4] S. Meyer, J. C. Leost, J. Guena, E. Penard and M. Goloubkoff, “Experimental Characterization of a 60 GHz Communication Channel Inside a Building”, International Symposium on Personal, Indoor and Mobile Radio Communications, Yokohama, Sep. 8-11, 1993

[5] L.M. Correia and P.O. Francês, “Materials Characteristics in the Millimetre Waveband”, COST 231 TD(93)065, Barcelona, May 1993

[6] J. Lähteenmäki and T. Karttaavi, “Transmission Coefficient Measurements of Building Structures at 60 GHz”, COST 231 TD(93)115, Limerick, Sep. 1993

[7] B. Langen, G. Lober and W. Herzig, “Reflection and Transmission Behaviour of Building Materials at 60 GHz”, International Symposium on Personal, Indoor and Mobile Radio Communications, The Hague, Sep. 21-23, 1994

[8] L. M. Correia and P. O. Francês, “Estimation of Materials Characteristics from Power Measurements at 60 GHz”, International Symposium on Personal, Indoor and Mobile Radio Communications, The Hague, Sep. 21-23, 1994

[9] J. D. Parsons, “The Mobile Radio Propagation Channel”, Pentech Press, London, 1992

8.7 Summary

Stephen Barton, University of Leeds, UK

After eliminating IR as a candidate transmission medium on grounds of eye safety in section 8.1.1, and finding mmw technology relatively mature and safe in section 8.1.2, the next three sections concentrated on mmw channel characterisation. In section 8.2 methods of characterising building materials at mmw based on scattering, bistatic reflection and transmission were described and the main electrical parameters of many common building materials tabulated. Also tabulated were the minimum thicknesses required for various degrees of isolation between rooms to control interference. Walls made from all materials except glass and plasterboard will provide sufficient isolation to enable re-use of the same frequency in every room.

Section 8.3 described narrow and wideband measurements, statistical and deterministic modeling of the mmw indoor radio channel. The narrowband measurements concern mainly DOA, which can be used to investigate individual signal paths. The results indicate that a gain of 8.4 dB can be achieved by using an adaptively steered antenna at the remote station. Wideband measurements in a variety of indoor areas with different shapes, dimensions and wall material were described. From the resulting time-domain data base, cell coverage and RDS under LOS and OBS conditions were derived. Values varied between 10 and 100 ns.

A statistical model for the power delay profile of the indoor mmw channel has been derived from the measurements. It consists of an LOS ray followed by a constant level part up to 60 ns, followed by a linear decrease (in dB). A deterministic model of mmw indoor radio propagation based on GO was also described. Computer simulations with various combinations of antenna characteristics showed that a setup with biconical horns at both ends yields NRP and RDS which are insensitive to LOS blocking and distance.

Section 8.4 described narrow and wideband measurements, statistical and deterministic modeling of the outdoor mmw channel. Here the Oxygen absorbtion is expected to limit cell radii to less than 1 km. The break point between inverse square law and fourth power law propagation is found to be at least 7 km, so that in all realistic situations a path loss exponent between 2 and 2.5 can be assumed. Wideband measurements and a ray-tracing model indicated that DS in city streets and tunnels would be in the 10 - 50 ns range while in open areas such as squares it could reach 100 ns or more.

Section 8.5 reviews the main types of transmission techniques which may be used to overcome the limitations of the wideband multipath dispersive channel. These are DSSS with a RAKE receiver, multicarrier or OFDM modulation, antenna diversity and adaptive equalisation. Studies of equaliser performance in the

Fig. 8.6.6 shows the throughput of a network of ten nodes with different numbers of hidden nodes. There are $10 \times (10 - 1)/2 = 45$ different possible connections [54]. The throughput rises to 0.85 for the fully connected network and remains at this level in the congested region. However, with increasing numbers of hidden node pairs the throughput is reduced. The main reason is that a node which is hidden from the current transmitter believes the channel to be free, and can therefore transmit asynchronously causing a collision at the receiver which can hear both.

The basic problem with these collision resolution protocols is that they rely on sensing the channel at the transmitter, whereas collisions occur at the receiver. One protocol has been proposed which does not suffer from this problem.

In the RTS/CTS protocol [54] data transmission is preceded by an exchange of short packets between source and destination nodes, see Fig. 8.6.7. The RTS and CTS packets contain source and destination addresses, and the length of the data packet which is to follow. Other nodes which hear either RTS or CTS defer for the length of the data packet. Any node which is might interfere with the data reception at the destination hears the CTS and defers, even if it is hidden from the source and cannot hear the RTS or the data. Unfortunately, the RTS/CTS protocol does not readily accommodate multicast or broadcast traffic. It is therefore included only as an option in the draft IEEE P802.11 standard.

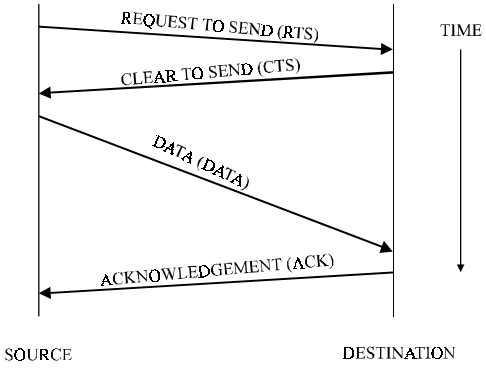

Fig. 8.6.7 RTS/CTS protocol

if the highest priority packet awaiting transmission is priority 3, all nodes with priority 3 packets transmit at the same time, i.e. after 30 μs.

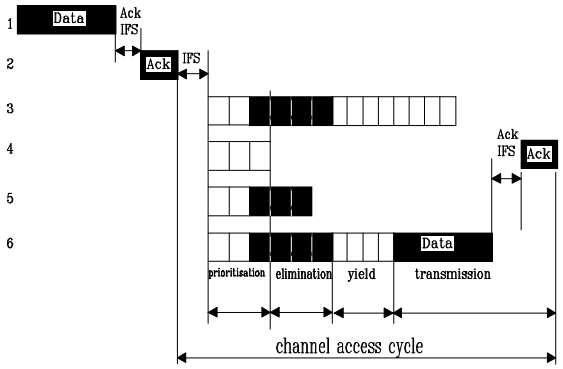

Fig. 8.6.5 EY-NPMA

In the elimination phase, all surviving nodes choose a random number of slots to transmit their elimination burst. At the end of its elimination burst a node must listen to check whether another node is still transmitting, in which case it defers until the next access cycle. The nodes which have chosen the longest elimination burst now move into the yield phase. Each surviving node now listens for a random number of slots. When the node which has chosen the smallest number of yield slots starts to transmit its data, any remaining survivors hear it and yield until the next access cycle.

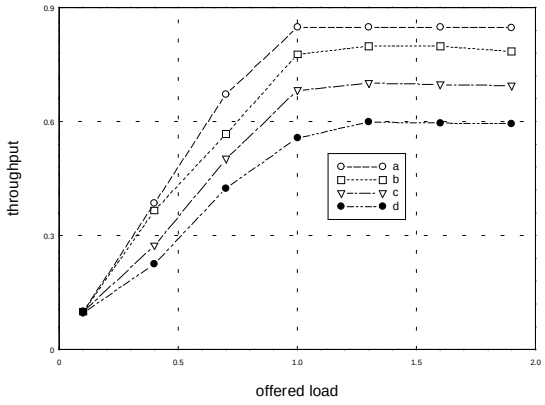

Fig. 8.6.6 Throughput with Hidden Nodes: a: fully cnnected, b: 1, c: 3, d: 5 pair of hidden nodes.

frequency. Thiu collision detection is not available, so alternative means of avoiding collisions must be found. Three approaches, referred to as the COMB-scheme, Elimination Yield Non-Pre-emptive Priority Multiple Access (EY-NPMA), and Request to Send/Clear to Send (RTS/CTS) are discussed below.

The COMB scheme [37] is based on collision resolution rather than detection. Each node precedes its transmission by a signaling period in which it switches between transmitting and receiving according to some random pattern of bits known as the comb, see Fig. 8.6.4. All users contending for access to the channel synchronize to the end of the previous transmission, and transmit during the first 'tooth' of the comb. Where two users both transmit or both receive in the same tooth, they will not detect one another. As soon as one transmits when the other is receiving, the receiving one detects the other and defers. In this way, given sufficient teeth in the comb, the number of contending users is reduced to one, which can then transmit its data.

The COMB scheme is claimed to be more efficient than CSMA/CD because collisions are resolved, allowing one node to transmit successfully, whereas in CSMA/CD both contending nodes cease transmission. However, it does rely on all nodes being able to receive one another, i.e. it does no accommodate hidden nodes. The requirement to switch rapidly between transmit and receive mode is also difficult for the radios to meet.

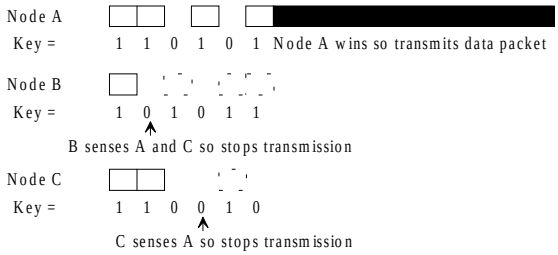

Fig. 8.6.4 COMB Scheme

The protocol which has been adopted for HIPERLAN, EY-NPMA [54] is a further development of the COMB scheme, requiring only a single signaling pulse to be transmitted before the data, and thus reducing the need for rapid switching of the radio between transmit and receive modes, see Fig.8.6.5.

All contending nodes are again synchronised to the end of the previous burst. The access cycle is divided into four phases: prioritisation, elimination, yield and transmission. In the prioritisation phase, nodes listen to the channel for a number of 10 µs slots depending on the priority of the packet awaiting transmission. Top priority packets wait 10 µs, lower priority packets 20 µs etc. If no node of higher priority asserts the channel during its listening period, a node may transmit the priority assertion pulse. Otherwise it must defer until the next access cycle. Thus,

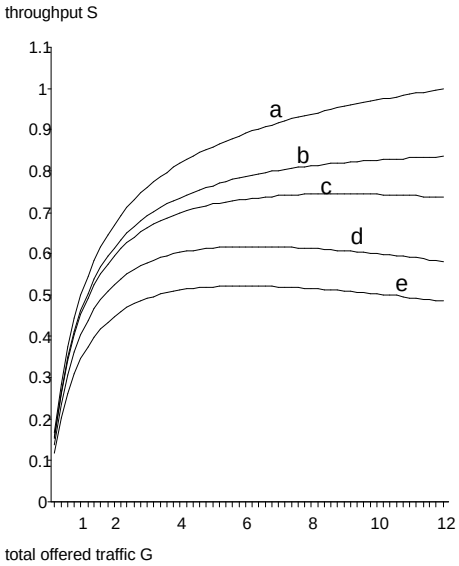

Fig.8.6.3 Throughput of slotted non-persistent ISMA, capture ratio = a: 0 dB, b: 2 dB, c: 4 dB, d: 6 dB, e: 8 dB.

8.6.3 Distributed Networks

In Ad-hoc networks there is no BS with overall control of access to the transmission medium. A node which happens to give access to the fibre backbone network is treated the same as any other. Communication is on a peer-to-peer basis and the network topology is Mesh. The lack of a central base station also means that there is no separation between up-link and down-link channels, so that a single channel is used for all traffic. This is no bad thing because typical LAN traffic is far from symmetrical, so that a fixed division of resources between up- and down-link traffic would be inefficient. It does introduce another problem for radio LANs, however, because a node cannot receive signals at -70 dBm from a distant transmitter at the same time as it is transmitting up to +30 dBm on the same

subtracted the number of permits for RS(i) currently waiting in the BS permit queue. In this way the possibility of a cell remaining permanently in the RS because either request or permit is incorrectly received is avoided. Each time a new permit is added to the queue the timer is reset to t(i). This is then decreased by one every timeslot until it reaches zero, when a new permit for RS(i) can be added to the queue. In this way the maximum rate for RS(i) is maintained at one cell per t(i) timeslots.

8.6.2 Centralized control based on random access

This section presents the throughput analysis of a random access protocol: nonpersistent inhibit sense multiple access (ISMA) in the mmw band for indoor communications. In random access protocols any RS may transmit whenever it believes the medium to be free, assisted by any side-information provided by the system. In a radio network a RS may not be able to detect the activity of another RS, even if it's transmit and receive frequencies are the same. This "hidden node" problem means that Carrier Sense Multiple Access, with or without Collision Detection (CSMA/CD) becomes unreliable. On the other hand, differences in received signal levels at the BS from different RSs leads to a capture effect, in which collisions do not necessarily cause the loss of both colliding packets. Providing the signal to interference (plus inter-symbol-interference plus noise) ratio exceeds the "capture ratio", denoted z_0, the stronger signal will be successfully received

In ISMA, the BS transmits inhibit bits on the down-link, indicating that the up-link is busy. The RS must wait until the inhibit bit is reset before it may transmit. This does not completely prevent collisions as two waiting RSs may start to transmit at the same time. This problem is mitigated to some extent by the nonpersistent random back-off algorithm. As with other contention based protocols, performance is further improved by a time slotting structure.

The performance of both slotted and unslotted non-persistent ISMA over an idealised mmw radio channel based on the results in section 8.3 above, and for various values of normalised RDS and z_0 is presented in [52],[53]. An example of the results is shown in figure 8.6.3. This shows the throughput of slotted np-ISMA over the LOS channel with Ricean K-factor of 0 dB on both up- and down-links, and RDS = 0.5, for five different values of z_0.

1) Permits for ATM cells. These (CL = 1) contain the address of one RS, indicating that it is allowed to send one ATM cell.

2) Permits for request blocks. These (CL = 0) contain the address of the next RS in the list. The permit entitles this RS, and the next five on the list, to send a short request packet.

The BS issues permits for request blocks whenever it has no permits for ATM cells to send. Therefore, the idle periods of the upstream traffic are used for transmitting request blocks. In this way, the spare upstream capacity is exploited to increase the reaction speed of the protocol to changing traffic situations. Fig. 8.6.2 shows the downstream traffic structure, both for permits for ATM cells and permits for request blocks.

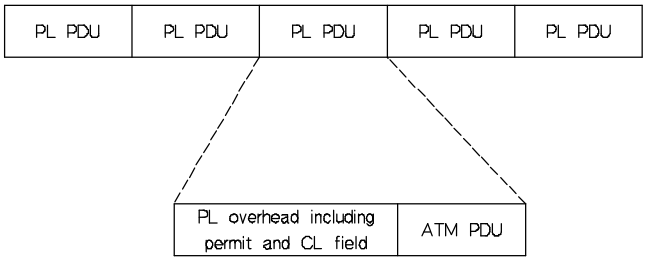

Fig. 8.6.2 Downstream information structure.

The main characteristics of the permit distribution algorithm are: 1) the peak bit rate per RS is enforced by spacing the cells, 2) a global FIFO discipline is used (over all RSs) to minimize cell delay variation and to achieve fair access, and 3) cells awaiting transmission are buffered in the RSs (distributed buffering).

To control the maximum allowed peak bit rate for each RS(i), the protocol enforces a minimum time spacing, t(i) between consecutive cells, inversely proportional to the peak bit rate agreed in an initial negotiation procedure between RS and BS. The number of new cell arrivals is deduced from the requests and the necessary permits are assigned to the RS. These permits are put into a FIFO queue together with permits for the other RSs with the constraint of minimum time spacing between two consecutive permits for the same RS. In this way, the actual queuing takes place in the RSs, while the central control in the BS maintains a permit FIFO queue, by which the transmission instants and the order in which the different RSs are emptied are governed.

The central controller maintains two counters per RS, one indicating the number of requests which have not yet been allocated a permit, and one indicating the time which must elapse before another permit can be granted to RS(i). The requests declare the number of cells currently waiting in the RS queue. From this is

call set-up, the protocol dynamically allocates the available upstream capacity. The RSs are then informed about the allocated capacity by means of permits.

Requests contain information about the number of ATM cells awaiting transmission in the local queue at the RS. Two types of requests are available:

1) Requests coupled to the upstream ATM cells. An RS which already has a permit to transmit a cell may attach a request to it.

2) Requests contained in dedicated request blocks. An RS which does not have a permit to transmit a cell must wait for the BS to declare a dedicated request block, and for its turn in the sequence to use these blocks.

Without the second type of request, an RS which had been inactive for a short time could never rejoin the system. The request blocks are the same length as an upstream cell, and contain[1] short request packets originating from a number of consecutive RSs.

Fig. 8.6.1 shows the upstream information structure. In this figure, a Physical Layer Packet Data Units (PL PDU) consists of a PL preamble including a request field and an ATM PDU, i.e., a standard ATM cell. The PL preamble may also include a field for error control, see [51],[16].

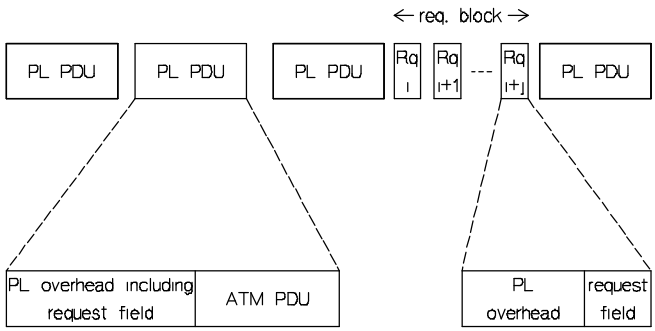

Fig. 8.6.1 Upstream information structure.

The protocol allocates the available capacity among the RSs by means of permits broadcast on the down-link. Permits are attached to downstream cells, which need not be addressed to the same RS as the permit. There are two types of permits, distinguished by a permit class bit, CL:

---

[1] A request block also contains a dedicated time slot in which a new station can send a request for registration. A randomised retransmission strategy is used to avoid persistent collisions and large retransmission delays. When the BS receives a request for registration it inititates a registration proceedure and allocates an address to the new RS.

multiplexed between them. In the second, a single encoder is used and the decoders operate on overlapping sections of the received data stream.

The required length of overlap depends on the code rate, E_b/N_0, and decision depth, and varied from a few bits to about 200. This was found not to be a major overhead as the block lengths could be up to 20,000 bits. Results of shortening the outer RS code, and RS symbol interleaving are also reported. The sufficient depth of interleaving is around 5–8 RS symbols, see fig. 8.5.8. Finally, no significant additional coding gain is expected from the decreased coding rate of a shortened RS code.

8.6 Network Performance Evaluation

Peter Smulders, EUT, Netherlands, Ramjee Prasad, DUT, Netherlands and Stephen Barton, University of Leeds, UK

A number of different network architectures and types of traffic have been considered within WG3. Access networks to a fibre backbone, which use radio only for the last 50m, will typically have a centrally controlled star architecture, with overlapping cell coverage areas accommodated by a frequency reuse pattern. In such networks all communication is between RS and BS, and either frequency (FDD) or time division duplex (TDD) can be used to separate the up- and down-link traffic. As with fixed networks, Medium Access Control (MAC) protocols based on demand assignment are better for networks with small numbers of nodes generating roughly constant traffic, while random access protocols are better for large numbers generating sporadic traffic. Ad-hoc networks, on the other hand, are essentially distributed in nature and therefore cannot accommodate any central control function, so random access protocols must be used. In this section a demand assignment protocol for access to the public switched B-ISDN network, a random access protocol for access to private computer networks such as FDDI, and some distributed protocols for ad-hoc networks are discussed.

8.6.1 Centralised control based on polling

Most efficient traffic throughput is provided by systems in which access to the medium is allocated centrally, provided the signalling overhead is not too great. Fairness is achieved by maintaining a unified queueing system in the central controller. A protocol based on access units matched to the standard 53-octet ATM cell, and proposed by Smulders and Blondia [50],[16] is described in this section.

It operates according to a request/permit mechanism as follows; each RS declares its capacity requirements by means of requests, which are sent to the master of the protocol located in the BS. Using these requests, together with parameters agreed at

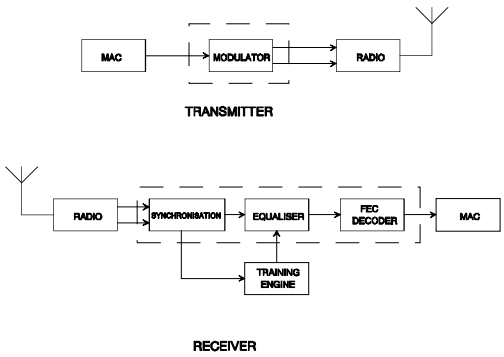

Fig. 8.5.7 System block diagram.

8.5.7 Channel coding

Ref. [48] discusses the requirements for error control in ATM-based indoor radio LANs. The maximum acceptable cell-loss rate varies from 10^{-5} to 10^{-9} according to the type of traffic. ATM is designed for fibre networks with very low BER and therefore has only end to end error control. Radio links require error control on a link by link basis to achieve the same cell loss rates. BCH codes capable of correcting one or two errors in a 511 bit block are considered, with and without a single re-transmission strategy (when uncorrectable errors are detected). It was found that dual antenna diversity was essential for all schemes to achieve the required transmission rates.

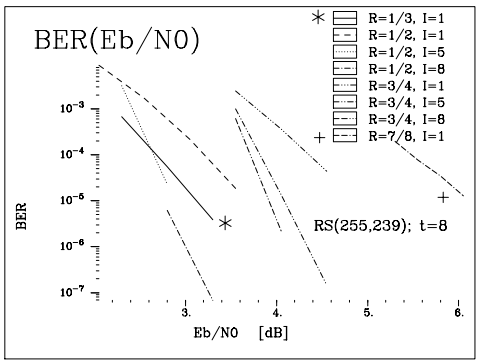

Fig. 8.5.8 The BER performance vs. E_b/N_0 for concatenated and multiplexed coding schemes (soft decision). R — the rate of convolutional code; I — interleaving depth.

Ref. [49] addresses an issue of Viterbi decoding of convolutional codes in the situation where the speed of a single decoder chip is too low and multiplexed decoders have to be used. In the paper, two methods of multiplexing low speed Viterbi decoders are compared. In the first, multiple encoders are used and the data

analysis shows that there is an irreducible outage probability which depends on the ratio of the rms delay spread to the equaliser span, see fig. 8.5.6.

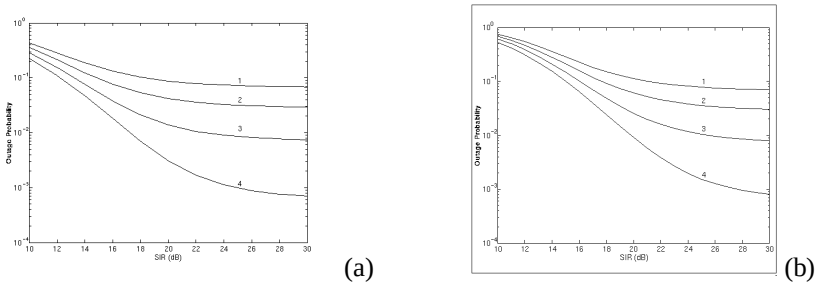

Fig. 8.5.6 Outage probability vs. SIR, simplified channel model, (a) single interferer, (b) two identical, independent interferers, RDS values: 1: 70 ns, 2: 60 ns, 3: 50 ns, 4: 40 ns.

Proposed modulation schemes for ESPIRIT project 7359, LAURA, emphasising the synchronisation and training/acquisition properties are described in [45]. Three different sequences are embedded in the data to indicate "start of burst", "end of burst" and at regular intervals for measurement of phase rotation rate (frequency offset).

Simulations of the performance of synchronisation codes optimised for recovering frame synchronisation in an asynchronous mesh network are described in [46]. Because HIPERLAN is intended to operate without a central control station, synchronisation must be recovered on a packet by packet basis, using synchronisation sequences. The packet loss rate is a function of the false acceptance and false rejection rates, which depend on the correlator output threshold. The steepness of the curves indicates that the threshold level, set by the automatic gain control (AGC), must be very accurate. A sequence length of at least 80 bits is required to achieve a packet loss probability of 0.5%.

Because a large part of the research presented within the WG3 activities was related to the HIPERLAN standardisation activities, several papers were also presented at COST-231 where either the HIPERLAN system proposed was presented in general, or where the implementational aspects of HIPERLAN were discussed. In [47] the signal processing hardware in the LAURA project is described, see fig. 8.5.7. The transmission rate is 15 Mbps. The GMSK modulator, synchronisation circuits, equaliser and FEC decoder are described.

In [41] a decision feedback equaliser (DFE) is considered and it is shown that the number of forward taps has a profound influence on the maximum normalised bit rate; an increase from 3 to 7 forward taps results in a maximum rate increase of about a factor of 5, as shown in fig. 8.5.5.

It could also be noted that a significant improvement of the maximum normalised bit rate (maximum bit rate multiplied by the rms delay spread) can be obtained by applying a high gain circular horn antenna at the base station or remote station instead of a biconical horn antenna. The best results are achieved if the remote is equipped with a circular horn.

8.5.6 HIPERLAN

In [42] the constraints on the choice of modulation scheme for HIPERLAN are described. First, requirements for the modulation scheme are discussed, such as: robustness to interference, low hardware complexity, constant envelope and amenability to low-complexity DFE structures. Some of these requirements arise from the peak envelope power restriction and the requirement for uncoordinated ad-hoc mesh networks. A steep spectral roll-off is required to accommodate four channels in 100 MHz bandwidth, and constant or near-constant envelope to avoid the need for highly linear amplifiers. Based on these criteria, two modulation schemes are selected: $\pi/4$ DQPSK and GMSK. It is concluded that the linearity requirements of $\pi/4$ DQPSK are too stringent for HIPERLAN, so continuous phase FSK is retained for further examination. Finally, GMSK modulation is shown to be a good compromise in terms of spectral roll-off and ISI.

In [43] the performance of the linear transversal equaliser (LTE) and the DFE is compared with the matched filter bound in a wide band tapped delay line that characterises the multipath fading in the indoor radio environment. Results show that the matched filter bound improves as the rms delay spread increases, and is virtually independent of roll-off factor. DFE is typically 2 dB and LTE 5 dB worse than the matched filter bound for the three delay spreads (50, 100 and 150 ns) considered by HIPERLAN. The performance of equalisation techniques for QPSK modulation with square root raised cosine filtering was evaluated using Monte Carlo simulations for the indoor channel. The channel impulse response consists of 128 independent taps with a uniform tap spacing of 7.8 ns. The ensemble average power delay profile is assumed to be exponential. Taking into account LTE, DFE and matched filter bound, the DFE closely follows the matched filter bound, and outperforms the LTE.

In [44] the effects of a finite equaliser span on the performance of a radio link in a delay spread channel are analysed. The equaliser is assumed to remove all ISI over a limited equaliser range of delays (its span). The residual ISI after the equaliser is combined with co-channel interference to produce a probability of outage, defined as the probability that the signal to interference ratio (SIR) falls below 10 dB. The

It was found that QC-combining shows superior performance enhancement compared to unity gain combining. A significant improvement of performance is achieved by QC-combining of a relatively small number of antenna signals, and small array dimensions. A four element antenna array requires a circle with radius of about $\lambda/2$, which is a relatively small area at high frequency. Its performance is nearly equal to maximal-ratio combining with a slight decrease in performance for low bit rates, however without the requirement of a priori knowledge of the channel impulse profiles.

8.5.5 Adaptive Equalisation

In [2] a preliminary evaluation of the capacity limitations on broadband indoor networks was carried out for a single carrier indoor radio link within a typical office environment (40 x 60 x 4) m^3 and reflectivity of each wall equal to 0.2. Within this room, mobile stations are communicating using antennas located a few decimetres above a table, whereas the base station antenna is located in the middle of the room just beneath the ceiling. All antennas have omnidirectional radiation patterns in the horizontal plane. The availability of the LOS path between the transmitter and the receiver was assumed. For this configuration the radio channel information capacity was calculated. Evaluation of indoor radio channel characteristics was based on power delay profile, i.e., magnitude squared of the complex impulse response of the channel. The target throughput of 30 Mbps (corresponding to a coded moving picture) was assumed. Under the assumption of the required bit error rate of 10^{-6}, 8 Mbps is achievable without an equaliser, 30 Mbps transmission is feasible with a 3-tap DFE equaliser, or even 70 Mbps transmission if a 7-tap DFE equaliser is used.

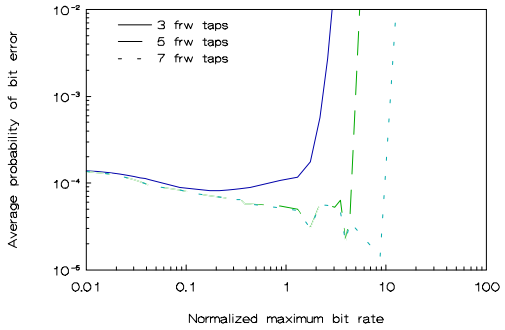

Fig. 8.5.5 Average probability of bit error versus normalised maximum bit rate for various number of forward taps, Room A.

combining requires a priori knowledge of the complex impulse response of the channel for each antenna element. A better result is achieved by Minimum Mean Square Error (MMSE) signal combining, however here also a priori knowledge of the channel's complex impulse response is required.

A way of combining multiple antenna signals which does not require a priori knowledge of the complex channel impulse responses for the different antenna elements was presented in [39]. The technique is based on quasi-coherent (QC) combining of the dominant path of the signals received by M different closely spaced antenna elements. Because of the small array dimensions, the channel PDP is nearly equal for all antennas. The M antenna signals are phase shifted so that the phases of the dominant path become nearly equal. Summation of these signals results in coherent addition of paths which arrive from the same direction as the dominant path. Signals which arrive from other directions will add incoherently. Therefore, the dominant path is strongly enhanced compared to other paths, and the resulting PDP shows less delay spread and consequently has a more equalised frequency response. Coherent combining, which is the optimum case for this scheme, requires exact knowledge of the phase of the dominant paths. However in a practical situation these phases are unknown and have to be estimated. Therefore, the term quasi-coherent combining is used.

The scheme of a coherent BPSK receiver with QC-combining of multiple antenna signals is shown in Fig. 8.5.4. Remodulation is applied for carrier phase recovery, by multiplying the delayed input signal by the estimated data. A delay time T_b is added to take into account the time required for optimum detection of $d(t)$. In case no errors are made, remodulation fully removes the modulation, and the result is a clean carrier signal from which the reference phase is determined. In case of errors, the fraction $(1-2P_e)^2$ of the total signal power is concentrated in the recovered carrier [40].

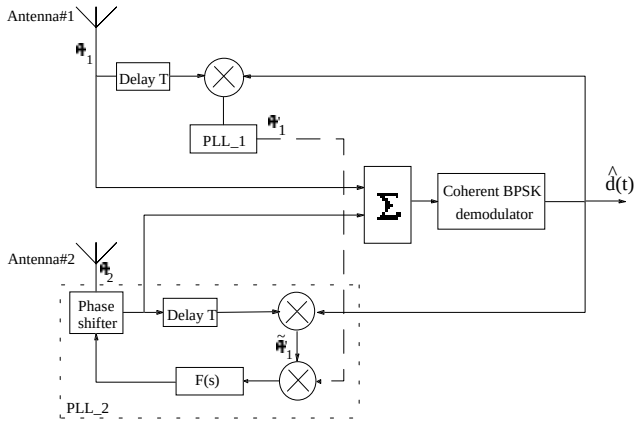

Fig. 8.5.4 Scheme of proposed BPSK receiver with quasi-coherent signal combining.

8.5.3. Multicarrier modulation

Several multicarrier schemes were proposed to ETSI RES-10 as candidates for the HIPERLAN standard, and are summarised in [37]. The main reasons for rejecting multicarrier schemes were connected with the high peak to mean power ratio. The spectrum was allocated by the regulators under the constraint of a maximum isotropically radiated peak envelope power of 1 W. This means that the average power is limited to 1W divided by the number of carriers unless the peak is limited, eg. by clipping, which leads to out-of band radiation. As HIPERLAN is intended for battery powered portable computers, it was desirable to use efficient Class-C power amplifiers and this effectively precluded multicarrier schemes.

A hybrid system incorporating multitone, DS and equalisation is studied in [38]. A bidimensional RLS (Recursive Least Square) linear equaliser is described. At high data rates, multipath propagation leads to ISI on individual carriers, and also cross-carrier interference (CCI). The equaliser is therefore a multiple input, multiple output bidimensional device. The structure can be simplified to a block diagonal matrix. Simulation results are presented for a system operating at 10 Mbaud in the 5.2 GHz band, using 1, 2, 3, 8 or 16 carriers in a channel with 50 ns rms delay spread, see fig. 8.5.3. A 7-bit m-sequence is used as a spreading code for the single tone system, with longer sequences for the higher number of carriers.

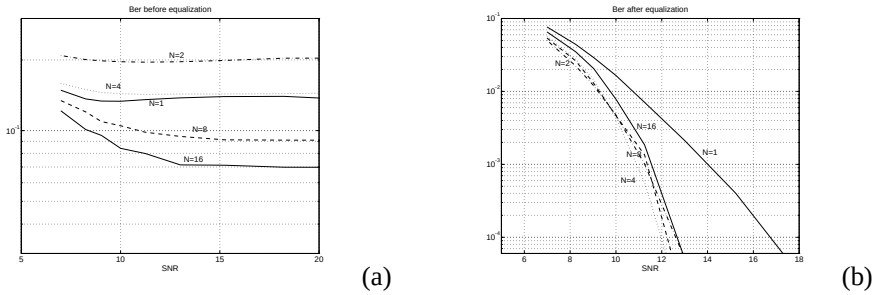

(a) (b)

Fig. 8.5.3 BER for DS-multitone without (a) and with (b) equalisation for different numbers of tones.

The positive effect of increasing the numbers of tones is demonstrated, especially when no equalisation is used. It is noted that the multitone effect is reduced by the equaliser and that convergence problems may arise when the number of tones is more than two.

8.5.4. Antenna Diversity

A well known way of antenna signal combining is maximal-ratio combining. This however, is a narrowband technique which is optimal for the flat fading channel and does not take into account intersymbol-interference (ISI). Maximal-ratio

classes of spread spectrum used in WLAN, Direct Sequence (DS) and Slow Frequency Hopping (SFH), are compared. The modulation scheme considered is differential BPSK. The interferer is considered as narrowband white noise source (narrowband in the sense that the interferer bandwidth is less than the signal before spreading or after de-spreading). The network topology considered is mesh (no base stations and therefore no power control). SFH is found to be more robust than DS in the presence of narrowband interference, see fig. 8.5.1, but only DS offers any advantage against multipath dispersion.

A DS system with a RAKE receiver is considered in [36]. The channel model used is a discrete exponential power delay profile truncated at 30 dB power decay with components at chip delay intervals. BPSK modulation is used with two demodulation schemes, differential and quasi-coherent, and three different methods of combining the RAKE branch outputs (signal strength selection, equal gain combining and maximal ratio combining).

An irreducible BER of 10^{-3} is achieved with normalised RDS up to 0.3, 0.7 and 0.9 for selection, equal gain and maximal ratio combining respectively, see fig. 8.5.2. This means that for 100 ns RDS, data rates of 3, 7, and 9 Mbit/s can be achieved. DS WLANs use the lowest possible processing gain in order to maximise the instantaneous data rate for the active terminal, typically using 11-chip Barker codes as spreading sequences. The bandwidth requirements for the systems above would thus increase to at least 33, 77, and 99 MHz. This processing gain is insufficient to withstand interference from other users, so CDMA is not possible, and the MAC protocol is required to control access to the channel.

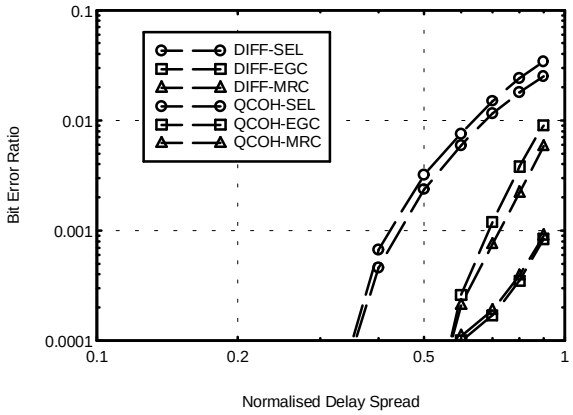

Fig. 8.5.2 Irreducible BER vs. NDS. DIFF: differential demodulation; QCOH: quasi-coherent demodulation; SEL: signal strength selection; EGC: equal gain combining; MRC: maximal ratio combining.

with the modulation index of $\beta = 2.0$ seems to offer the best performance. The results show that, with a significant line-of-sight path present (LOS $\geq$ 10 dB), the performance of the 8-ary GFSK system subject to 15 dB signal-to-co-channel interference (S/CCI) ratio and with 13 dB SNR can achieve bit rates up to 100 Mbps in large rooms, with as much as 90 ns rms delay spread, without the use of adaptive techniques. The general conclusion is therefore that for systems with a line-of-sight present (or one dominant reflected component) bit rates of 100 Mbps can be achieved in quite large rooms by using suitable modulation techniques (especially wideband GFSK), without the need for diversity or adaptive equalisation.

In [34] wideband measurements in eight indoor locations are described. The objective was to examine the propagation characteristics of mmw indoor radio channels. In each area, measurements were performed for 20 randomly chosen positions of the remote antenna. Gray-coded QPSK modulation was used, without any equalisation. The normalised bit rate (maximum bit rate, averaged over 20 locations, and multiplied by the rms delay spread) was calculated for the threshold value of BER = 10^{-6}. Finally, it was noted that the normalised bit rate values do not depend significantly on the considered indoor area and the type of antennas.

8.5.2 Spread spectrum

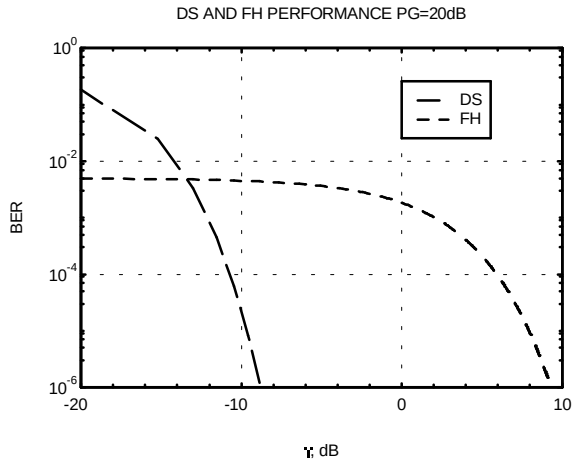

Fig. 8.5.1 DS and SFH performance, 20 dB processing gain; γ: signal to interference ratio.

Early Wireless LAN products operated at about 1 Mbit/s in the Industrial Scientific and Medical (ISM) bands around 902 - 928 MHz and 2.400 - 2.4835 GHz and used spread spectrum to avoid interference. It was therefore logical to investigate whether these techniques could support higher data rates. In [35] the two major

8.5 Transmission Performance Evaluation

Witold Holubowicz, EFP, Poland, Peter Smulders, EUT, Netherlands and Ramjee Prasad, DUT, Netherlands

The most important characteristic of the radio channel for high speed data transmission is the RDS. Multipath dispersion produces an irreducible BER which is independent of the signal to noise ratio and increases with increasing RDS. Where no countermeasures are taken, as a rule of thumb, an irreducible BER of 10^{-3} results from a normalised RDS of 0.1. This means that the maximum useable transmission rate is 0.1/RDS. For 100 ns RDS, this is only 1 Mbit/s. There are four main countermeasures that may be considered: Direct Sequence Spread Spectrum (DSSS) with a RAKE receiver, multi-carrier techniques such as Orthogonal Frequency Division Multiplex (OFDM), Antenna Diversity, and Adaptive Equalisation. All of these techniques have been considered in WG3, both singly and in various combinations, but equalisation has received most attention. This section addresses each of these techniques in turn, leading to further elaboration of the equaliser approach in the context of the HIPERLAN standard. It ends with some material on synchronisation and channel coding for wideband systems.

8.5.1. Early Performance Predictions

In [32], the design of a wireless indoor transmission chain with 10 Mbps bit rate at about 30 GHz is described. Different techniques are discussed that allow such high rates to be achieved within buildings: proper choice of multiple access method, use of higher level modulation, adaptive equalisation, antenna diversity, and frequency diversity. First, a comparison between CDMA and narrow-band transmission is carried out. It is shown that for the spreading factor of at least 250 and 20 users each transmitting at 10 Mb/s, the transmitted signal would have too large spectrum and the spread spectrum approach was therefore not further pursued. A more promising approach, according to the authors, was a single-channel-per-carrier (SCPC) FDMA system for the uplink and multicarrier FDM for the downlink. Apart from the mobile-to-base and base-to-mobile connections, another layer of radio links is also assumed: between the base stations and one central station in the company. Different solutions for communication in that layer, based on demand-assignment SCPC/FDMA are also proposed. According to the authors the system proposed is a good compromise between spectral efficiency and relatively low cost.

In [33] the authors present results of simulation and analyses concerning indoor signal transmission in the presence of co-channel interference from the adjacent room in the one cell per room scenario. The performance of MPSK, narrowband GFSK (B = 0.5) and wideband GFSK (B = 2.0) is considered. Error performance is calculated for exponential PDP models in the presence of co-channel interference modelled as AWGN. Amongst the modulation systems considered wideband GFSK

Results (CIR) from this tool were checked against measurements [30] showing that this approach is correct. Fig. 8.4.3 shows a comparison of results for one of the streets, street 'A' which has trees both in the middle and on the sidewalks. In general good agreement is observed, with the exception of the 90% SDW. This can be understood as this parameter is very sensitive to reflected rays with low amplitude, therefore presenting large differences between model and reality.

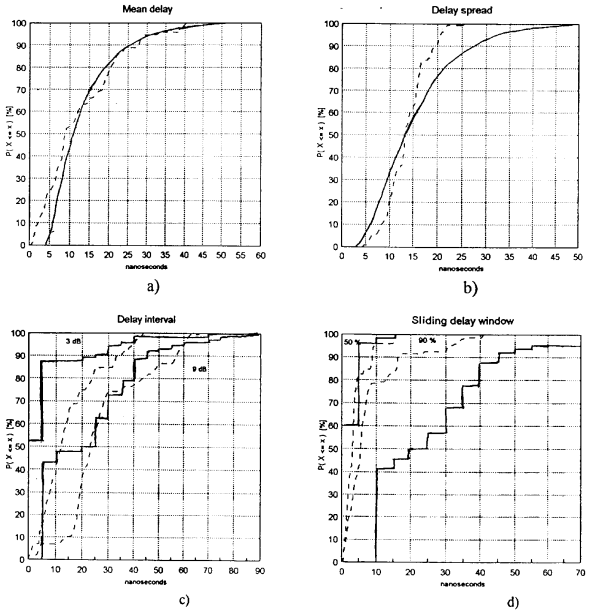

Figure 8.4.3 Comparison between ray-tracing and measurements, of statistical parameters (___ measurements; _ _ _ simulations)

One of the main conclusions is that simple ray-tracing can be used to estimate channel characteristics, both for narrow and wideband systems. Several improvements are being considered for further study, such as the inclusion of motor traffic.

receiver antenna, all vertically polarized with vertical half power beamwidth of 20^{o}. The height of the receiver antenna in all outdoor measurements was 2.2 m, and the transmitter antenna height was generally around 4 m.

Results from these measurements are summarized in Table 8.4.2. 50% and 90% values from cumulative distributions of the channel parameters are tabulated. In Figure 8.4.2, 'street A' scenario is shown together with a sample of an impulse response.

For outdoor scenarios the main conclusion is that city streets do not normally represent a severe multipath situation, values of DS and 90 % SDW being typically lower than 20 ns and 50 ns respectively. The dimensions of a city square, typically being larger than the city streets, result in a much larger dispersion. In this case, the 90 % SDW may be 150 ns or more. A road tunnel represents a very homogenous situation and has many similarities to the city street environment. A parking garage represents a bad multipath situation because of the large dimensions and the relatively smooth surfaces creating strong reflections.

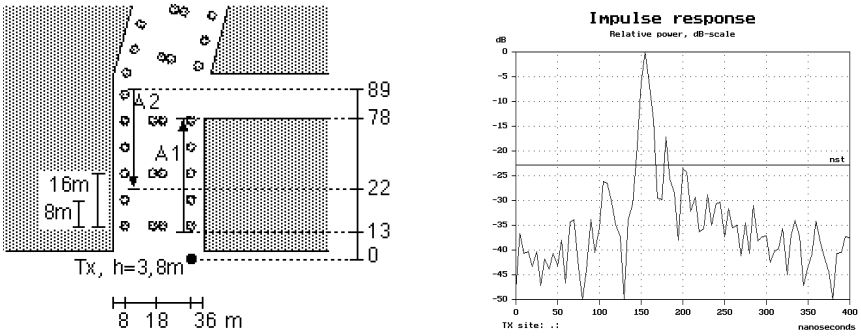

Figure 8.4.2 Street plan and sample CIR for 'street A' (circles represent trees; arrows A1 and A2 represent mobile movement; shadowed areas are buildings)

Besides the model for the average received power, a model for characterization of the signal in terms of fading depths and duration and of wideband parameters (MD, DS, etc.) is needed. A ray-tracing tool was developed [31], with the following main features: it accounts for direct and reflected rays (up to the third order), neglecting diffuse reflections and diffractions; rays are interrupted by non-reflecting objects like trees (measurements have shown that diffuse reflection from trees is negligible).

The scenario is described as a dielectric canyon, having rough surfaces. Polarization and radiation patterns of both transmitting and receiving antennas are taken into consideration. This tool, more complex than the previous ones, is intended to simulate signal behaviour in outdoor scenarios, more specifically in urban streets, allowing the estimation of both narrow and wideband channel characteristics.

shortest portion of the CIR containing a certain percentage of the total energy, which is believed to be a better measure than DW, e.g. when judging equalizer performance.

Rte.	Scen.	Env. W	Env. C	MD [ns] 50%	MD [ns] 90%	DS [ns] 50%	DS [ns] 90%	9 dB DI [ns] 50%	9 dB DI [ns] 90%	90% DW [ns] 50%	90% DW [ns] 90%	90% SDW [ns] 50%	90% SDW [ns] 90%
A1	ST	36	s	10.2	13.7	7.6	16.5	10	25	20	35	10	25
B1	ST	23	s	7.8	10.5	4.2	6.5	5	20	10	20	10	20
C	ST	20	n	9.3	16.1	8.4	13.1	15	35	20	40	15	30
D	ST	19	f	9.0	14.2	6.8	11.8	15	30	20	35	15	30
E	ST	14	f	5.7	11.1	3.6	12.6	5	20	10	35	10	20
F	ST	13	m	6.5	20.6	3.6	48.3	10	35	10	80	10	40
G	ST	27	m	6.2	11.4	4.6	16.0	5	20	10	50	10	20
H1	SQ	100	f	22.5	65.5	31.9	55.2	25	130	95	155	55	125
H2	SQ	100	f	11.5	39.1	20.1	60.2	5	135	10	160	10	140
I	SQ	70	f	17.3	62.2	28.1	76.6	10	150	55	195	15	150
J1	SQ	100	s	17.4	49.2	40.8	92.2	5	150	45	270	10	135
J2	SQ	100	s	19.5	57.0	37.8	83.7	10	200	90	220	15	160
K1	T	15	m	10.9	17.1	6.8	11.5	15	30	20	35	15	30
N	G	67	n	37.0	74.6	38.4	61.2	40	160	115	175	55	145

Table 8.4.2 Main figures from the wideband measurements (Scenario: ST = street, SQ = square, T = tunnel, G = garage; Env.: W = width of street or tunnel, or largest dimension of city square or parking garage, C = moving cars: n = none, f = only a few, s = some, m = many).

The measurement campaigns that started early 1994 include wideband channel soundings and wideband path loss measurements in city streets and squares in downtown Oslo, a road tunnel and a parking garage, [29], [30]. A 90^{o} horn was used as transmitter antenna in all measurements, and a biconical horn was the

Rain can play an important role in cell coverage reduction, since its attenuation can reach values larger than those of oxygen, depending on the rain rate (18 dB/km for 50 mm/h). Oxygen and rain attenuations cannot be neglected if large distances (~1 km) are to be considered, but for calculations within cells (with ranges less than 200m), they may not be of great importance.

The average received power can be estimated by combining the expressions of almost free space received power with the attenuation by oxygen and rain. Thus the total received power is given by:

$$P_r = P_t + G_t + G_r - 32.4 - 10\alpha \log(d) - 30\alpha - 20 \log(f) - \gamma_r d - \gamma_o d \qquad (8.4.5)$$

where P_t is the transmitted power (dBm), G_t, G_r are the transmitter and receiver antenna gains (dBi), and d is the distance (km). The value for α has to be chosen with some care, depending on the specific application intended for the model. This expression cannot be used for very small distances where the antenna radiation patterns will have a great influence. This model agrees very well with the data from [23], giving a maximum 2 dB error in the estimation of the received power. Comparison with the data from [24] also leads to good results. However, note that the measurements in Table 8.4.1 have a maximum range of 200 m. There is a need for more measurements over a larger range, to check the model for distances up to 2 or 3 km (necessary at least for interference calculations).

8.4.2 Wideband Characterisation

When designing the air interface, reliable information about the propagation conditions is of vital importance. Since little work had previously been published on propagation measurements in the mmw band, measurement campaigns with a 60 GHz channel sounder were performed by Telenor R&D. A channel sounder based on correlation, transmitting a digitally generated frequency sweep, was assembled [28]. The received signal is digitized and stored, and then correlated with a Taylor weighted version of the transmitted sweep. Diversity measurements are possible, since the input from two antennas can be synchronously sampled. Several hundred impulse responses per second may be transferred to the PC, or the receiver may calculate delay-Doppler spectra based on successive responses and transfer these spectra to the PC. The RF center frequency is 59.0 GHz, with a maximum bandwidth of 200 MHz, corresponding to a best resolution of 5 ns. The output transmit power is 500 mW.

The basic wideband measurement is the channel impulse response (CIR) which is a time function of the received signal, showing the arrival times of the different radio paths. This type of measurement is very well suited to describe multipath phenomena. From the CIR measurements several parameters may be extracted, and they may have different significance when describing the channel or for the design of a mobile system. Mean delay (MD), delay spread (DS), delay interval (DI), and delay window (DW) are defined in [9]. A new delay window parameter, the sliding delay window (SDW) was introduced, defined as the length of the

for choosing the 60 GHz band. Other factors can affect wave propagation, but they are not considered here: water vapour absorption can be neglected, since its attenuation coefficient is of the order of 0.1 dB/km; fog, hail, snow, sand, etc. are not very well studied, but their influence can also be neglected, either because the attenuation coefficient is very low, or because they occur with very low probability.

Scenario	Gain [dBi]		Height [m]		d [m]	α
	Tx	Rx	Tx	Rx		
Open area (grass) [23]	20	6	1.5	1.5	200	2.3
Open area (asphalt) [22]	17	15	5.	1.5	200	2.0*
Open area [21]						2.2*
Urban Street [22]	17	15	5.	1.5	120	2.2*
Campus street [24]	6	20	1.5	2.	120	2.1
				5.5	120	2.3
Tunnel [22]	17	15	1.5	1.5	200	2.5*

Table 8.4.1 Power-distance decay rate at mmw in outdoor scenarios (* -- estimated from figure)

An expression for the oxygen absorption has been developed, based on [26]

$$\gamma_o(f) = \begin{cases} 15.10 - 0.104(f - 60)^{3.26} & (60 \le f \le 63) \\ 11.35 + (f - 63)^{2.25} - 5.33(f - 63)^{1.27} & (63 \le f \le 66) \end{cases} \quad (8.4.1)$$

Where f is the frequency in GHz. This specific attenuation due to oxygen, γ_o (dB/km) can take relatively high values at 60 GHz (around 15 dB/km), but it decreases an order of magnitude when the frequency is near 66 GHz. This decrease must be taken into account when the frequencies are chosen for the up and down links, especially if the distances are greater than 1 km.

Rain attenuation can also be of some importance at the mmw band, depending on the rate, R (mm/hr). The model given by ITU-R [27] is used,

$$\gamma_r(f, R) = k(f)\, R^{a(f)} \quad (8.4.2)$$

where γ_r (dB/km) is the specific attenuation due to rain, k(f) and a(f) are approximated by:

$$k(f) = 10^{1.203 \log(f) - 2.290} \quad (8.4.3)$$

$$a(f) = 1.703 - 0.493 \log(f) \quad (8.4.4)$$

Simple ray-tracing tools have been developed [21], [22], accounting only for direct and reflected (up to the second order) rays; scenarios were considered to be as simple as possible, neglecting any objects (for instance streets are considered as dielectric canyons). Comparisons of measured and simulated results, of which Fig. 8.4.1 is a good example, show good agreement indicating that reflections of third order, or higher, and diffraction can be neglected, as far as modeling the variation of power versus distance is concerned.

According to simulations, frequency or space diversities mitigate fading effects, decreasing the fade depths by several dB. Selective combining of two or more frequencies (with a separation of the order of 1 GHz) shows that diversity is more effective for lower frequencies (10 GHz compared to 60 GHz). Selective combining of signals from two antennas separated by 1 m (much more than the correlation length at mmw) show similar improvements.

The models used at UHF for the decay of power with distance usually have the slope dependent on the environment and on break-point distances. They are very simple models based on the interference of a direct and a ground reflected ray, leading to a simple dependence of the power on distance d, of the type $10\ \alpha \log(d)$, α being the decay slope. It is well known [9] that a two ray model leads, under conditions that are usually verified, to a fourth power law, rather than the square law found in free space. One of the conditions to be satisfied is that the path length difference between direct and reflected rays is less than $\lambda/2$, which defines the break-point distance, $d_{bp} = 4\ h_t\ h_r/\lambda$ (h_t, h_r being the receiver and transmitter antenna heights) beyond which the fourth power law can be used. Such a model for the mmw band requires the evaluation of the break-point distance, and an environment classification according to the different values of α. Assuming a frequency range [60, 66] GHz, and h_r = 1.8 m, $h_t \in$ [5, 50] m, $d_{bp} \in$ [7.2, 79.2] km, which is far beyond the expected maximum range for the cell radius (up to 0.5 or 1 km). This means that it is not expected to have the fourth power law at mmw band, and that α will be close to that of free space (α = 2), which is confirmed by the few results from measurements available in the literature, see Table 8.4.1.

The value of α does not seem to depend only on the scenario, since a value of 2.3 is found in an open space as well as a street. The range in which α varies is not very large [2, 2.5]. The antenna height seems to influence the value of α (but note also the influence of the radiation pattern, when the antenna is very high). The value of α will, of course, be of greater importance for larger distances, since larger values of α contribute to a faster decay of the power.

The model developed for the mmw band (60 - 66 GHz) [25] includes two additional terms, compared to the UHF band, besides the usual term related to the slope of the power decay with distance: one to account for oxygen absorption and the other for rain attenuation. These terms are negligible in the UHF band, but cannot be neglected for higher frequencies. Moreover, oxygen absorption is the main reason

Measurements play an important role in propagation modelling at all frequencies, being of extreme importance at the mmw band since there are not many results in the literature, and the relative importance of many phenomena need to be clarified by an experimental procedure. Therefore, measurement campaigns were undertaken in different outdoor scenarios (streets, open squares, highways, tunnels, airports, etc.).

8.4.1 Path Loss Modeling

Estimation of power for coverage or interference calculations is essential in every mobile system. At the UHF band several types of models have been developed, using different approaches, from which two categories can be considered: 1) decay of the average power with distance, depending on several parameters of the system and environment (like base station antenna height or street width), and 2) ray-tracing on 3D models of the scenarios under analysis, demanding a very accurate knowledge of the characteristics. These approaches have also been used at the mmw band.

Both narrow and wideband measurements have been conducted in several outdoor scenarios in the mmw band. Initially, narrowband measurements of power versus distance were performed [21], [22] in scenarios chosen so that very different cases were considered: airport field, urban street and city tunnel. In all cases, results show an interference pattern, typical of those associated with the sum of several rays, suggesting that ray-tracing techniques can be used to model the propagation phenomena. Results were compared with ray-tracing tools.

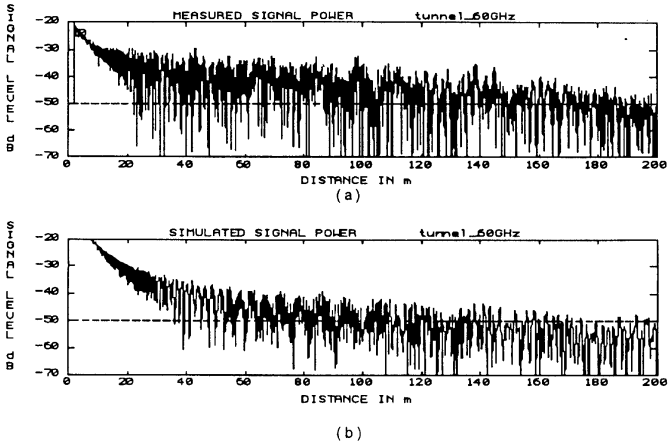

Figure 8.4.1 Comparison between measured (a) and simulated (b) power in a city tunnel at 60 GHz.

maximum values for NRP and RDS for the sec-bic setup are not so extreme. The spread in NRP values is significantly lower.

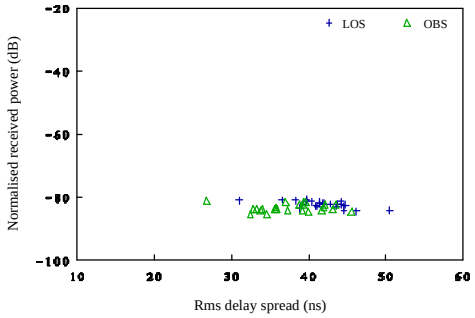

Fig. 8.3.13 Results for the low reflective room with bic-bic setup under LOS and OBS conditions.

With respect to the bic-bic setup, in contrast with the sec-sec and sec-bic setup, an increase in antenna directivity yields an increase of the RDS values. Fig. 8.3.13 depicts the results obtained with a 9 dBi biconical horn at each end for both LOS and OBS. The differences in NRP values between those two cases are only a few dB. This indicates that the bic-bic setup is highly insensitive to LOS obstruction. Furthermore the low spread in NRP values is striking. It demonstrates that with the application of properly dimensioned biconical horn antennas, an almost uniform coverage within the boundaries of an indoor cell can be achieved.

This phenomenon is explained by the fact that for larger separation distance, the corresponding larger free-space loss is compensated by the elevation dependence of the radiation patterns [18]. The similarity between LOS and OBS and uniformity in coverage is also found for the highly reflective room with slightly higher worst-case values of about 55 ns RDS and -72 dB NRP.

8.4 Outdoor Radio Channel

Luis Correia, IST, Portugal, and Per Lehne, Telenor, Norway

The use of the mmw band in an outdoor environment has been proposed for mobile applications, eg. car to car and fixed roadside cell to car communications, and communication between TV cameras and a central control room [20]. Particular interest has been devoted to the oxygen absorption band, [57,63] GHz, where the specific attenuation is greater than 11 dB/km, thus limiting the cell radius to a few hundreds of meters, and enabling efficient frequency re-use. The work carried out on propagation modelling concerns two different topics: path loss modelling, for the estimation of cell radius and carrier-to-interference ratio, and impulse response modelling, for evaluation of the wideband radio channel characteristics.

radiation beam of the sectoral horn at the RS. In the bic-bic setup both biconical horn antennas are radiating in the horizontal direction.

With respect to the sec-sec setup it could be observed that 25.1 dBi sectoral horns at both ends yield the lowest RDS values and the highest NRP values when compared with the other configurations, provided that there is no obstruction of the LOS path and the antenna beams are exactly pointing towards each other. The sec-sec setup is however highly sensitive to LOS obstruction and mispointing. This is illustrated in Fig. 8.3.11 and Fig. 8.3.12, respectively. which show the NRP versus RDS for every position of the remote station. The combination of LOS obstruction and 5° mispointing results in a fairly uniform spread in RDS and NRP. A higher reflectivity of the walls results in higher NRP values as well as higher RDS values.

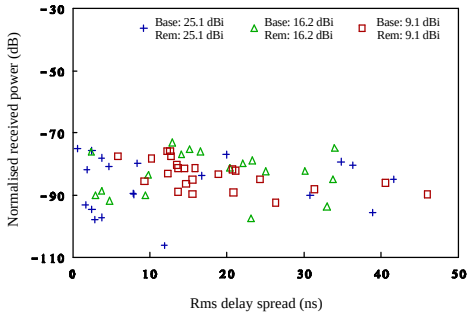

Fig. 8.3.11 Results for the low reflective environment with "sec-sec" setup and obstructed LOS.

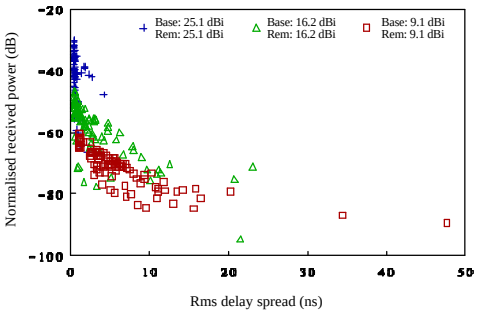

Fig. 8.3.12 Results for the low reflective environment with "sec-sec" setup and 5° pointing error.

As with the sec-sec setup the bic-sec setup is sensitive to obstruction of the direct ray and mispointing. The difference with the sec-sec results is however that the minimum and

The antennas implemented in PROSIM are smooth walled sectoral horn antennas and biconical horn antennas. In contrast with the omnidirectionally radiating biconical horns, sectoral horns produce highly directive radiation beams. To examine the influence of directivity antennas are implemented with various values. The directivity of the biconical horns was in the range 6.9 to 12.7 dBi whereas the directivity of the sectoral horns ranged from 9.1 to 25.2 dBi.

Simulations were performed for the three different antenna setups depicted in Fig. 8.3.10. Fig. 8.3.10a shows the antenna setup with a sectoral horn at both the RS and BS, denoted as "sec-sec". Fig. 8.3.10b depicts the "sec-bic" setup with a sectoral horn at the RS and a biconical horn at theBS. Fig. 8.3.10c shows the "bic-bic" setup with biconical horns at both the RS and BS.

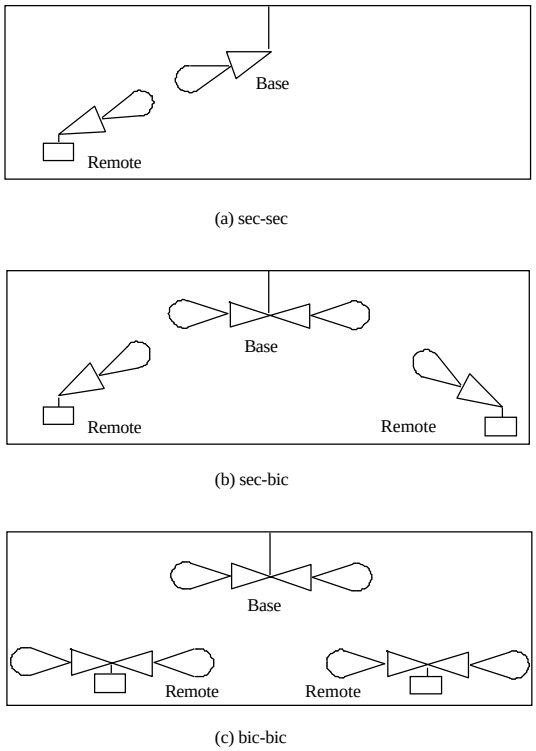

Fig. 8.3.10 Simulated antenna setups.

The sectoral horns in Fig. 8.3.10a are pointing towards each other, eventually with a certain amount of mispointing in order to examine the effects of pointing errors. The orientation of the error angles at the RS and the BS are mutually independent and randomly chosen. In the sec-bic setup the sectoral horn at the RS is pointing towards the biconical horn. Here, pointing errors are only introduced in the

8.3.4 Deterministic modeling

Ray-tracing programmes are used extensively for the examination of radio propagation characteristics. In order to investigate the propagation characteristics in an indoor environment various algorithms were developed taking into account the effect of transmission through walls and polarization. More sophisticated techniques have also been developed incorporating the effects of diffraction.

For simulation of the indoor propagation of mmw, the simulation package PROpagation SIMulation (PROSIM) has been developed at the Telecommunications Division of the EUT. The basic algorithms and procedures underlying the simulation package are based on Geometrical Optics (GO). This means that the ray-tracing algorithm applied traces possible rays between transmit and receive antenna according to Snell's reflection law.

Calculation of mmw propagation on the basis of GO yields a good compromise between accuracy and complexity [19]. Using GO means that ray paths are calculated along which electromagnetic power travels from transmitter to receiver. Fresnel reflection coefficients are applied, electromagnetic field polarization states considered and rays weighted with the radiation patterns of the transmit and receive antennas. PROSIM only considers the reflectivity of walls and objects (eg. furniture) but not the transmissivity. The walls (and windows) of the room are assumed infinitely thick and the objects within the room do not allow an electromagnetic wave to travel through them. The room and the objects within are represented by smooth faces. Objects are assumed to stand on the floor and can be arbitrarily orientated with respect to the horizontal plane.

Antenna directivity functions can be entered in formula form or stored in a look-up table. The latter enables the use of measured data without data reduction. Two types of aperture antennas are considered: 1) sectoral horn antennas and 2) biconical horn antennas. Radiation patterns of both these antennas are stored.

With the biconical horn antennas the accuracy of the applied GO model has been examined by comparing simulation results with measurement results, and good agreement found [19]. The use of PROSIM was continued for a more thorough examination of the influence of the environment and antenna characteristics on NRP and RDS.

The relation between NRP and RDS and the shape and orientation of antenna radiation beams has been evaluated under both LOS and OBS conditions. To examine the influence of wall reflectivity two rooms are considered having dimensions similar to those of Environment A. One room has low reflective walls (10 dB return loss at perpendicular incidence) whereas the second room has walls with high reflectivity (1.5 dB). In both rooms the BS receive antenna is located at 3 m height in the middle of the room and the RS transmit antenna is placed at 1.4 metres height at 24 randomly chosen positions throughout the room (as with the measurements). For every position of the RS antenna the impulse response was calculated. The NRP and RDS were derived from each obtained profile.

excluded that have amplitude values more than -20 dB below the highest ray amplitude.

In calculating the average power delay profile (PDP), each individual PDP is weighted by its normalized received power value. This is done because a single PDP should not dominate in the average PDP. Three examples of average PDPs are shown in Fig. 8.3.9. These profiles have been obtained in the environments F,G and H. They are typical for all measurement subsets obtained. A typical PDP can be modelled by a LOS ray followed by a constant-level part up to τ_t = 60 ns which in turn is followed by a linear decrease (of dB value) down to the noise floor.

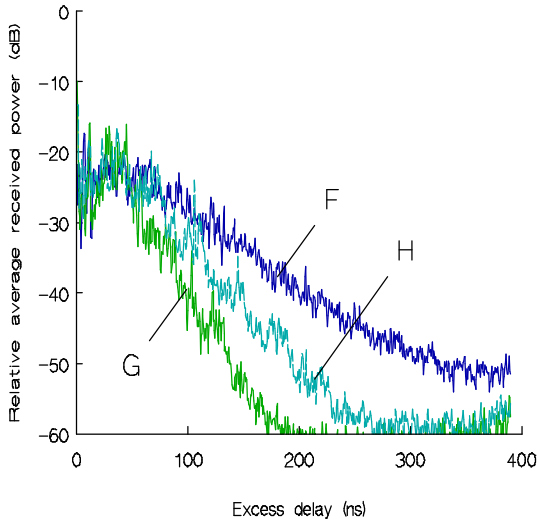

Fig. 8.3.9 Example of an average PDP.

The normalized received power of the LOS component can be calculated using the radio equation. OBS situations can be modelled by completely omitting the LOS component. The constant level part is caused by the elevation dependence of the antenna radiation patterns and the height difference between the transmit antenna and receive antenna. The pulses in a response that immediately follow the first pulse (LOS pulse) are likely to come from single reflected rays. This suggests that the difference between the height of the first LOS pulse and the height of the constant-level part is determined by the average return loss of the dominant wall partitions.

The complex equivalent lowpass impulse response of a millimetre wave indoor radio channel can therefore be considered as discrete.

It is assumed that the amplitude statistics of reflected rays follow a Rayleigh distribution. This assumption was verified with a goodness-of-fit test, conditioned on the event that a ray exists. LOS rays were excluded. Data values that are not recognized as reflected rays are not taken into account and each detected ray is represented as a single point having a particular amplitude and excess delay in the impulse response. With this approach a meaningful amplitude distribution for each measurement subset is obtained since each resulting sample set contains only "non zero" ray amplitudes. Hence the test can be utilized to model the ray amplitude generation process independent from the ray arrival process.

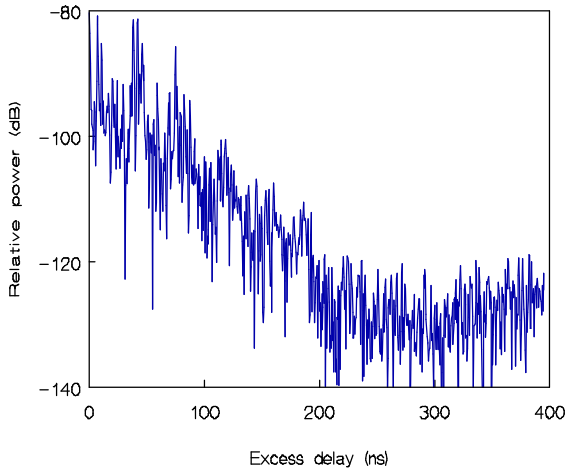

Fig. 8.3.8 Example of measured impulse response.

A reasonable assumption for the ray phases is that they are mutually independent random variables which are uniformly distributed over [-180°,180°]. This follows from the fact that the ray phase is critically sensitive to the path length, changing by 360° as the path length changes by a wavelength, or only a few mm. The assumption of uniformly distributed ray phases was checked for all measurement subsets and found to be true.

The interarrival time pdf's were subjected to a MMSE test. (A chi-squared goodness-of-fit test failed to yield significant results because of the limited number of interarrival time classes). Good correlation coefficients between exponential fit and empirical frequency distributions were found. The mean interarrival time is most reliably characterised as being 1 to 3 ns with the proviso that those rays are

decay rate exponent were typically much smaller (<0.5) than those reported for indoor UHF radio channels. This is because this parameter is not only determined by the LOS-distance, but by the antenna-gain function in elevation as well [18].

Fig. 8.3.7 shows the cumulative distribution functions of rms delay spread (RDS) values for both LOS and OBS-situations. Rms delay spread values tend to increase with the increasing reflectivity of the walls. Rms delay spread values in the small Environment F with metal walls (0 dB return loss) are even larger than in the large environment B with concrete walls (2 dB return loss).

Furthermore it is clear from Fig. 8.3.7, that the rms delay spread is fairly independent of the separation distance within each environment. Blocking of the direct path does not necessarily imply that rms delay spread has to increase; slightly higher and lower values for OBS-situations are observed in Fig. 8.3.7. Values between 10 ns and 100 ns have been found.

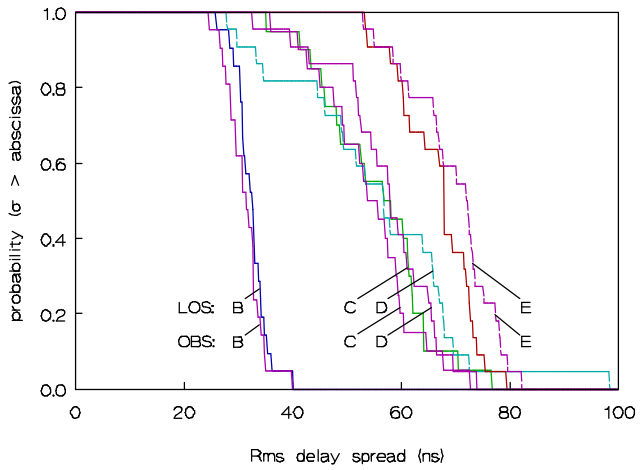

Fig. 8.3.7 Cumulative distributions of RDS in large rooms, hall and corridor.

8.3.3 Statistical Modeling

The measurement results can be used to describe the indoor radio characteristics in terms of statistical distributions and moments of the details of the complex equivalent low-pass impulse response. In Fig. 8.3.8 an example of an observed low-pass impulse response is shown (magnitude only). Individual rays could be detected by blocking the associated ray by an absorbing mat, while other rays were not noticeably influenced. This shows that a millimetre wave indoor radio channel is essentially a multipath channel. Hence, millimetre waves are sufficiently small to be modelled as rays following discrete paths.

The wideband measurements were carried out in eight different indoor environments at the Eindhoven University of Technology, denoted A to H, see table 8.3.1. Each consists of a single room, corridor, or hall, because millimetre waves are severely attenuated by most inner walls. In each room at least one series of measurements at 57-59 GHz was conducted at randomly chosen positions of the RS throughout the room. The RS transmitting antenna height was 1.4 m above the floor. The BS receiving antenna height was 3 m. The BS was placed in the centre of the room. Both antennas were levelled horizontally at every measurement position. The impulse responses were measured at about 20 positions of the RS, with the BS fixed, in each environment.

Owing to the difference in height between the RS and BS antennas, the path loss is partially compensated by the antenna radiation pattern in elevation. Hence; the received power does not depend significantly on the horizontal position of the RS.

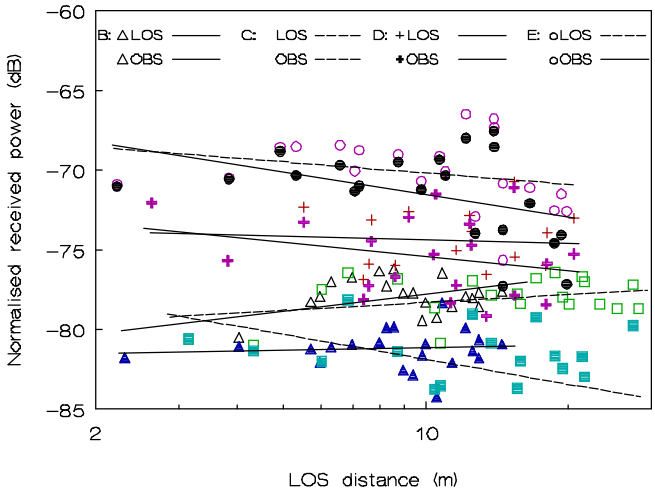

Fig. 8.3.6 NRP in the large rooms, hall and corridor.

Fig. 8.3.6 shows scatter plots of the normalized received power (NRP) versus separation distance for both line-of-sight (LOS) and obstructed (OBS) situations in the large rooms, hall and corridor. The values for OBS are derived from the time-domain data base under LOS conditions by mathematical removal of the direct ray. This method is justified by the experience that blockage of the direct ray by a person or cabinet caused a total drop of the LOS ray. The lines are linear fits based on the minimum mean square error. High values are found for environments with highly reflective (metal) objects and metal walls, while relatively low values are found in environments with only low reflective materials like wood. The fact that differences in received power between LOS and OBS-situations are only small (a few dBs at maximum) indicates that coverage is maintained under the circumstance that the direct LOS-ray is blocked. Measured values of the power-distance

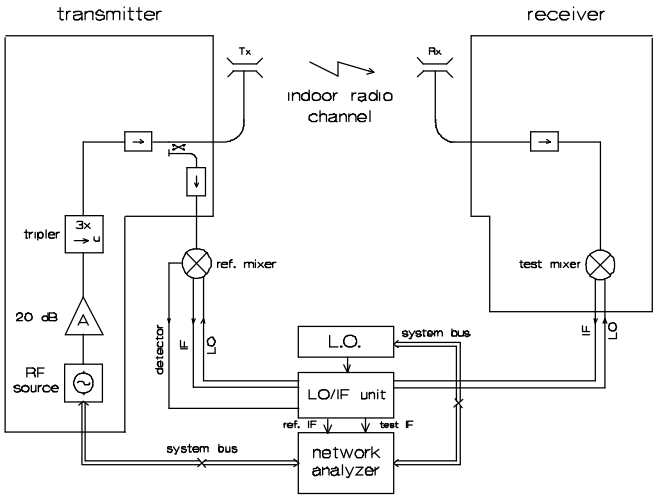

Fig. 8.3.5 Setup for wide-band measurements

The impulse response of an indoor radio channel is greatly influenced by the type of antennas used. These should be regarded as part of the indoor channel. For the experiments two identical biconical horn antennas were constructed, based on a design described in [18]. These antennas exhibit an omnidirectional radiation pattern in the azimuth plane and a torroidal beam in the elevation plane. The 3 dB elevation beamwidth was 9°, and the directivity 9 dB.

Room	Dimensions (m)	Shape	Comments
A	24.3×11.2×4.5	Cuboid	Empty, 1 glass wall, others wood
B	30.0×21.0×6.0	Amphitheatre	Cushioned chairs
C	43.0×41.0×7.0	Complex	Plastered concrete walls, ceiling
D	33.5×32.2×3.1	Complex	Metal computer cases
E	44.7× 2.4×3.1	Corridor	Metal walls, empty
F	9.9× 8.7×3.1	Cuboid	One side glass, others metal
G	12.9× 8.9×4.0	Cuboid	One side glass, others wood
H	11.3× 7.3×3.1	Cuboid	One side glass, others plaster

Table 8.3.1 Wideband Measurement Environments

Measurements at 60.5 GHz have been performed by France Telecom CNET [13] at 22 positions on a 1 m grid in an empty room with dimensions 6×4.7×3 m^3, see figure 8.3.4. Using a narrow beam antenna and a rotating positioning system at the receiver, DOA results and wall reflection coefficients were found. For all measurements, the height of the transmit and receive antennas was 1.5 m. A wide beam antenna, having a 3 dB aperture around 70°, was used at the transmitter. At the receiver a narrow beam antenna with 3 dB aperture close to 4.4° on a 2D rotating system was used. Measurements were made at 1° intervals so that every DOA could be found.

The direct ray is clearly dominant for each receiving position in the room. The number of significant rays depends on the receiving position. For positions in the middle of the room, the number of significant received rays is important. For these cases, contributions arrived from each wall in the room with about the same path lengths. In addition, because of the larger beam transmit antenna, each wall received direct contributions coming from the transmitter. Hence the situation is ideal for multipath propagation.

At other positions the number of significant rays is less. Where the receiver was close to walls, only the first order reflection is significant. The path length of second and third order reflections are specially large for these positions. Finally, for positions where the transmitter was not sighted directly towards the closer walls and the path lengths of all reflected rays are very long, second and third order reflections can be significant.

8.3.2 Wideband Measurements

The main purpose of wideband measurements is to characterise the dispersive nature of the radio channel, in order to dimension the equalisers that will be needed to overcome these effects. It is also useful, however, for taking signal strength measurements which are not subject to deep Rayleigh fading. Many techniques exist for wideband measurements, but for the indoor application, where distances are small and the channel can be made static, swept frequency measurements are invariably used. This permits much wider bandwidth, and hence finer delay resolution, than any other technique.

The system for performing the wideband measurements was built up around the HP 8510C vector network analyzer, which performs the frequency-domain measurements of the complex channel transfer function. The network analyzer controls an RF source which steps through the frequency range from 57 GHz to 59 GHz in 801 equally spaced steps. The resulting alias-free range in the time-domain is therefore (801-1)/(2 GHz) = 400 ns. A schematic diagram of the setup is depicted in Fig. 8.3.5. With the applied Kaiser window a time-domain resolution of 1 ns was achieved.

Figure 8.3.3 shows results derived from the Doppler spectrum technique of Deutsche Telekom. Note that the pattern is symmetrical about the path taken by the antenna, but only one of each par of lobes represents a real path. This is because the technique can only measure the angle from this line and therefore the direction can lie anywhere on a cone.

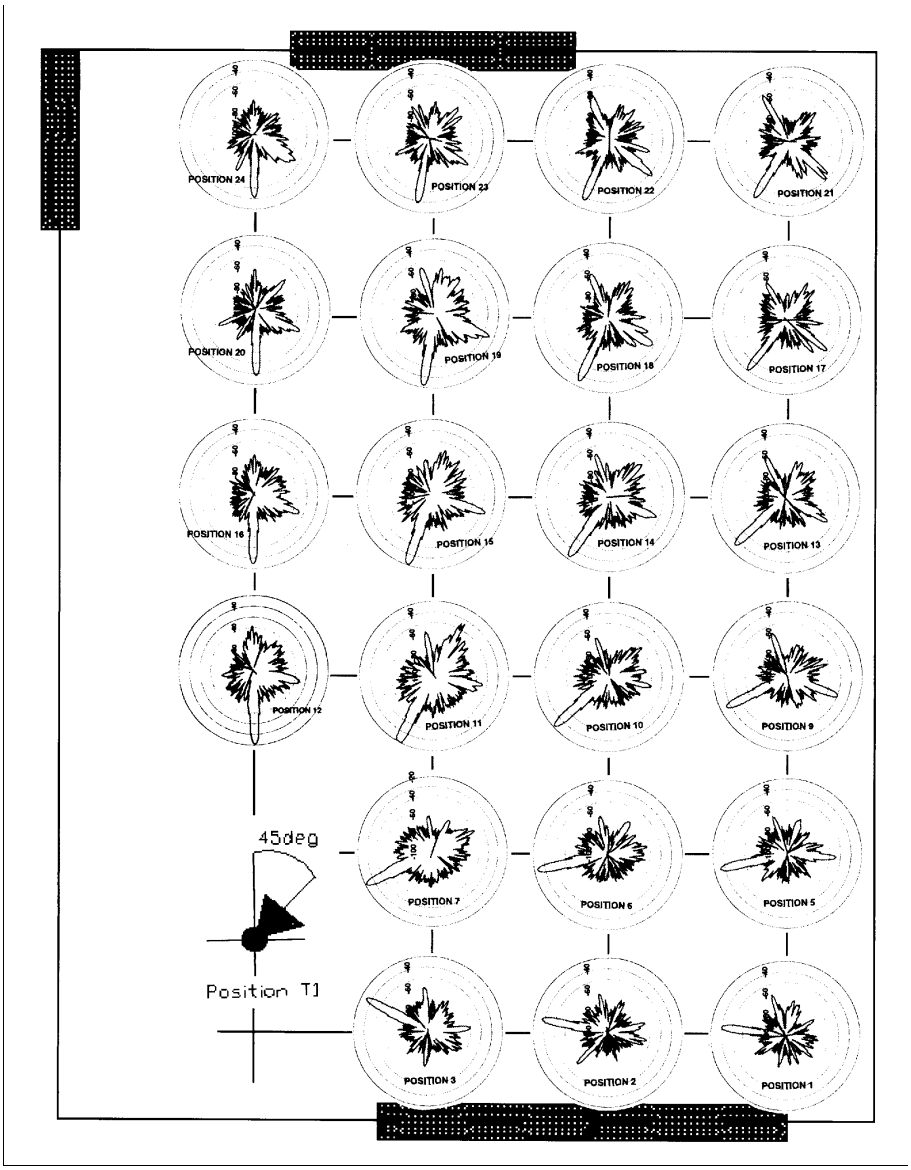

Fig. 8.3.4 Measured DOA distributions, 10dB/circle (CNET).

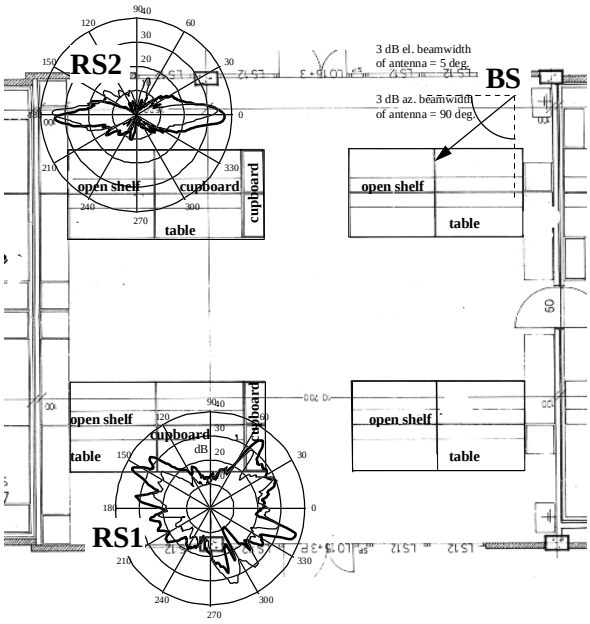

Fig. 8.3.2 Measured DOA distributions in a laboratory.

The level of link improvement achievable by using antenna steering in the azimuth plane can be estimated by calculating the DOA pattern gain. The gain is calculated by dividing the maximum peak of the pattern by the average received power.

According to 27 measured DOA patterns the gain is better than 8.4 dB for a probability level of 90%.

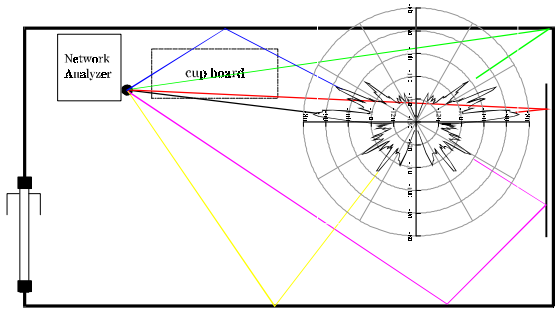

Fig. 8.3.3 Direction of arrival from Doppler Spectrum

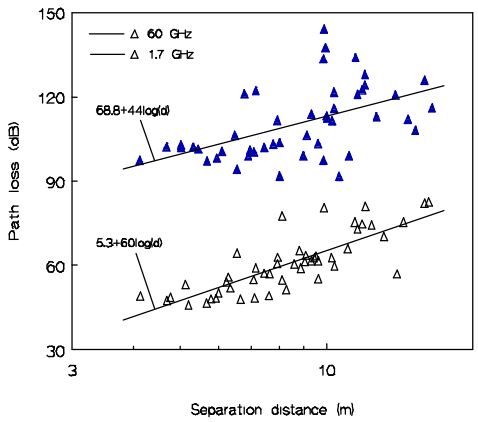

Fig. 8.3.1 Path-loss versus distance at 1.7 and 60 GHz.

Direction-of-arrival (DOA) measurements have been performed by TUE, VTT, and CNET using the same type of measurement system, but with a different antenna at the RS. This antenna has a narrow beamwidth (5°) in both vertical and horizontal planes. The antenna is rotated through 360° while path loss between the RS and BS is measured. Deutsche Telekom, on the other hand, used a synthetic aperture approach with an omni-directional antenna moving along an accurately defined track [17]. The DOA data can be used to investigate individual signal paths and to assess the advantage that can be achieved by using the steered high-gain antenna. If the DOA pattern shows distinctive peaks it is clear that the path loss can be reduced by steering a high gain antenna towards the maximum peak.

Typical measured DOA distributions in a room of size 11×13×3 m^3 in a laboratory room are shown in Fig 8.3.2. in the room there are open shelves with metallic supporting structures and cupboards entirely made of wood. The DOA plots consist of two lines. The thin line corresponds to a measurement in which the RS antenna is rotated in the azimuth plane. The thick line refers to a measurement in which the RS antenna is slightly elevated so that it is pointed directly at the BS antenna. Sliding average has been applied to remove fast fading.

At the point RS1 the direct path is blocked by a cupboard which introduces an additional loss of about 20 dB to the signal. It can be seen that the signal consists of several paths of the same order of magnitude. It is interesting to note that the signal level in any direction is very sensitive to the vertical orientation of the antenna. Therefore, manual or automatic steering of the antenna in both vertical and horizontal planes is useful in a real system implementation.

At the point RS2 there is a direct line-of-sight between the antennas. In this case only two dominant signal paths can be identified: the direct path and the wall reflected path. The reflected path is in this case very strong because the wall contains metallic plates.

One may conclude that for indoor systems the same frequency can be used in all rooms, assuming that there will be no glass or plasterboard walls to separate them, in which case different frequencies will be needed. Co-channel interference between indoor and outdoor systems will always be a problem, since glass is generally used in buildings (at least for windows), and the usual thickness of this material is not enough to isolate the two environments.

8.3 Indoor Radio Channel

Peter Smulders, EUT, Netherlands and Stephan Guérin, CNET, France

Indoor propagation measurements have been reported to WG3 by Technical University of Eindhoven (NL) [15], [16], VTT (Finland) [12], Deutsche Telekom [17] and France Telecom [13], and simulation results by the universities of Eindhoven, Ulm (D) and Aveiro (P). The bulk of this section is based on [16], which represents by far the largest contribution.

8.3.1 Narrowband Measurements

Narrowband measurements are not able to discriminate the multipath dispersion in the time domain, and are therefore limited to path loss and direction of arrival measurements. Path-loss measurements at 60 GHz have been performed with a CW source and spectrum analyser. The radiation pattern of the measurement antennas was narrow in the vertical plane (3 dB beamwidth = 5°) and broad in the horizontal plane (3 dB beamwidth = 90°). This kind of configuration is appropriate for a wireless LAN concept.

Results in an office building are shown in Fig. 8.3.1. Results from the same environment and the same distance range at 1.7 GHz have been included to highlight the differences between the two frequency bands. All the measurements are performed with base station (BS) and remote station (RS) on the same floor. The direct path is typically blocked by furniture or a light internal wall. A clear line-of-sight path is present only in few of the measurements.

In Fig. 8.3.1 it can be seen that the path loss is considerably higher at mmw. One reason for this is the antenna radiation pattern which introduces excess attenuation at short distances. Even at higher distances (15 m) where the excess attenuation is small, the difference between the two frequencies is rather high: 45 dB. Free space difference (31 dB) explains this result partly. The rest of the difference, 14 dB, is due to higher penetration loss of materials as well as higher reflection and diffraction loss at mmw. It can also be seen in Fig. 8.3.1 that the variance of data is proportional to frequency. The rms error at mmw is 11 dB while at 1.7 GHz it is only 6.3 dB. This is due to more severe shadowing effects at mmw.

calculate minimum thicknesses for given values of isolation. The relative weight of the two terms of the approximate expression for the attenuation depends on the polarization of the incident wave, the incidence angle ψ and the wall thickness ℓ. The first term, αs, does not depend very much on ψ ($s/\ell \in [1, \sqrt{\varepsilon_r/(\varepsilon_r-1)}]$ when $\psi \in [0, \pi/2]$), but is proportional to ℓ. On the other hand the second term, $-20 \log |1 - \Gamma^2|$, does not depend on ℓ, but shows a strong dependence on ψ (approximately $\in [0, \infty]$ for parallel polarization and $\in [-20 \log (4\sqrt{\varepsilon_r}/(\sqrt{\varepsilon_r}+1)^2), \infty]$ for perpendicular polarization). Thus, the isolation may be expressed [14] as

$$I_W\,[\mathrm{dB}] = \alpha \ell \qquad (8.2.5)$$

which takes into consideration that the second term can be 0, as well as the fact that s is of the order of ℓ (the maximum value of $\sqrt{\varepsilon_r/(\varepsilon_r-1)}$ is 1.732 for the materials considered here).

Type of material	ℓ_I [cm]		
	10 dB	20 dB	40 dB
Stone	1.75	3.49	6.98
Marble	8.00	16.00	32.00
Concrete	1.50	3.00	6.00
Aerated concrete	2.70	5.41	10.81
Tiles	1.28	2.56	5.12
Glass	1.65	3.31	6.61
Acrylic glass	9.71	19.42	38.83
Plasterboard	6.62	13.25	26.49
Wood	2.37	4.74	9.48
Chipboard	1.94	3.88	7.77

Table 8.2.2 Wall thicknesses for specific values of isolation

The values of wall thickness, ℓ_I, that ensure 10, 20 and 40 dB isolation are presented in Table 8.2.2. For an isolation of 10 dB one can already use the approximate expression for the attenuation for the cases referred to before. Again one can see that, with the exception of glass, acrylic glass and plasterboard, all the other materials will isolate at least 20 dB when they have the usual thicknesses in building walls and floors.

Parameters ε_r, tan (δ) and α are independent of the slab thickness, and have been estimated from measurements. Both R and T correspond to direct measured values and have a very strong dependence on the slab thickness, the values given here being for the usual thicknesses of materials in real buildings, to give an idea of their order of magnitude. This is not a complete list, and many more materials (especially composite cases) can be found in the references [11-14].

Later on, direction of arrival measurements were performed [12], [13]. In this case, the receiver antenna (with a very narrow horizontal beam width) is rotated through 2π, resulting in a "receiver radiation pattern" with lobes associated with incoming rays reflected from walls. By comparing the magnitudes of the incoming rays with their path loss, estimates of reflection coefficients for the real room walls were obtained. From these, values for ε_r and tan (δ) were calculated, which agree with those presented in the table.

8.2.3 Isolation and Transmission of Building Materials

Applications for the 60 GHz band are foreseen for both indoor and outdoor environments, which may pose interference problems. This suggests that the isolation as well as transmission properties of building materials should be evaluated, to facilitate coverage and interference calculations.

The attenuation suffered by a plane wave when going through a wall can be expressed as: $A_W = -20 \log |\tau_g|$. Three terms can be identified:

1) αs comes from the attenuation of a wave propagating in the slab,

2) $-20 \log |1 - \Gamma^2|$ is related to the transmission coefficients of both surfaces, and

3) $-20 \log |1 - \Gamma^2 e^{-j2ks} e^{-2\alpha s} e^{jk_0 d \cos(\psi)}|$ is associated with the internal reflection phenomenon. The relative weight of these terms is not the same, and in particular it is interesting to obtain the conditions in which the last term can be neglected, that is to say, when it is not necessary to consider the internal reflection phenomenon, the attenuation then being given by

$$A_W\,[\mathrm{dB}] = \alpha s - 20 \log |1 - \Gamma^2| \qquad (8.2.4)$$

Correia and Francês [14] have estimated the material thicknesses that enable the use of this approximate expression, for the average values of ε_r and tan (δ) presented in table 8.2.1. It can be used for almost all the materials with their usual thickness, the exceptions being glass, plasterboard and acrylic glass, for which thicknesses much larger than the usual values are needed.

For cell planning and interference purposes the isolation (ie the minimum value of attenuation, independent of polarization or incidence angle) provided by building materials is required. For this reason, it is important to establish a criterion and to

algorithm was used, increasing or decreasing alternately the value of ε_r or tan (δ), until the root mean square error between the measured and modeled values is minimised.

A different approach was taken in [6]. Transmissivity measurements were performed for a structure involving two slabs. The transmission coefficient of the double slab structure, as a function of the distance between the slabs (d_s) is approximated as

$$\tau = |\tau_g|[\ 1 - |\Gamma_g|^4/2 + |\Gamma_g|^2 \cos(2kd_S + 2\arg(\Gamma_g))| \qquad (8.2.3)$$

It is clear from this approximation that when the distance ranges in a given interval the transmissivity will oscillate between two values. From this, the values of ε_r and α were estimated by fitting the measured results to the expression. The results of all these measurements and estimations are summarized in Table 8.2.1. It should be noted that: ranges of variation are given each time more than one value has been obtained, either because different polarizations were used, or because they correspond to the results of different groups. The values presented here show a good agreement with others presented in the literature, e.g. [11].

Material	ε_r	tan (δ)	α [dB/cm]	R [dB]	T [dB]
Stone	6.72/8.55	0.005/0.066	0.67/9.39	-7.1/-6.0	-25.8/-2.8
Marble	11.56	0.007	1.25/5.00	-5.0	-4.8
Concrete	6.14	0.049	6.67	-8.2/-5.6	-35.0
Brick	--	--	4.00	-9.5/-5.1	-28.0
Aerated concrete	2.26	0.045	3.70	-14.0	-18.9
Tiles	4.01/8.58	0.023/0.091	3.70/9.94	-12.4/-3.8	-6.2/-5.7
Glass	4.70/6.13	0.033/0.082	4.05/9.97	-15.2/-1.4	-4.7/-2.1
Acrylic glass	2.52	0.012	1.03	-7.4	-0.9
Plasterboard	2.60/3.08	0.014/0.018	1.30/2.00	-16.7/-2.0	-3.9/-1.4
Wood	1.50/1.64	0.060/0.068	4.52/5.99	-16.1/-8.2	-13.0/-6.6
Chipboard	2.78/3.15	0.049/0.057	4.50/6.00	-15.2/-10.1	-13.9/-5.3

Table 8.2.1 Characteristics of building materials at mmw

$s = t/\sqrt{1 - (\cos^2(\psi)/\varepsilon_r)}$.

The path length difference on the slab of two consecutive departing reflections or transmissions is $d = 2\,t/\sqrt{(\varepsilon_r/\cos^2(\psi)) - 1}$.

With this model, reflected and transmitted powers from the dielectric slab will then be given simply by

$P^r = |\Gamma_g|^2\, P^i$ and $P^t = |\tau_g|^2\, P^i$,

P^i being the power of the incident wave; since it is assumed that the material is lossy, one has $P^r + P^t < P^i$. Although this model assumes that the slab is infinite, it can be expected that the results will be acceptable if the material sample is wide enough (compared with the intersection of Fresnel's first ellipsoid). Also it will contribute to a better approximation of this model to the physical reality if the losses are not very low, in order to make negligible the power carried by the waves that should propagate outside the real slab material, compared to the ideal slab.

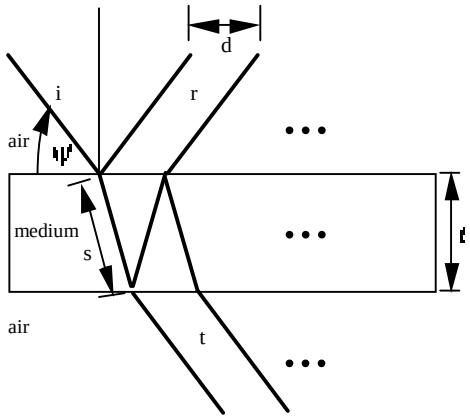

Fig. 8.2.2 Multiple reflections within a slab

The approach taken in [8] was to derive the parameters from the generalized reflection and transmission coefficients. These can be expressed as functions of the type $\Gamma(\psi, f, \varepsilon_r, \tan(\delta))$, $\Gamma_g(\psi, f, \varepsilon_r, \tan(\delta), t)$ and $\tau_g(\psi, f, \varepsilon_r, \tan(\delta), t)$. Measurements are taken at as many different values of ψ as desired. The problem of deriving ε_r and $\tan(\delta)$ then reduces to the resolution of a non-linear overdetermined equation system. There is no exact solution for this kind of problem. One approach is to use a least-squares method [10] in which several implementations can be used, all based on an iterative procedure. Some of them, although offering a faster convergence, require the evaluation of derivatives, which makes them very heavy from the computational point of view. Thus, a simple

8.2.2 Measurement Results and Parameter Estimation

Several groups within WG3 were involved in materials characterization in the 60 GHz band, using one of the measurement procedures described above. Initially reflectivity [3] and transmissivity [4] measurements were conducted. However, these results did not allow the estimation of the electromagnetic parameters, and a literature survey [5] has shown that values for ε_r and $\tan(\delta)$ were known only for glass and wood. Thus, measurements allowing the estimation of parameters were conducted: transmissivity for different slab thicknesses [6]; scattering and transmission patterns, and bistatic reflection measurements [7], [8]. Since it is not possible to extract the values of ε_r and $\tan(\delta)$ directly from the measurements, a model is needed.

The phenomenon of reflection of a plane wave by a perfectly flat infinite surface separating two indefinite media is well known, and can be described by a pair of reflection coefficients, according to the wave polarization. The reflection coefficients Γ can be found in many text books (e.g. [9]); they are a function of the incident angle (to the surface plane) ψ, and of the refraction coefficient of the medium n, which can be expressed by $n^2 = \varepsilon_r - j\,\varepsilon_r \tan(\delta)$. When the material thickness is large (compared to the wavelength) and/or the material losses are high, the reflection of a plane wave on a dielectric slab can be approximated by the reflection coefficient referred to above. However, when these conditions are not satisfied, this simple model can lead to significant errors, and a better model is necessary. The model that leads to a better approximation, and yet is not too complicated, is the one based on successive reflections of plane waves, as indicated in Fig. 8.2.2. With this model, the reflected field can be expressed by a generalized reflection coefficient, Γ_g, given as the addition of the simple reflection coefficient (from the first reflection) with the sum of a geometric progression corresponding to the reflections and transmissions inside the slab

$$\Gamma_g = \Gamma(1 - (1 - \Gamma^2)\, e^{-j2ks}\, e^{-2\alpha s}\, e^{jk_0 d \cos(\psi)}/\Delta) \qquad (8.2.1)$$

and a generalized transmission coefficient, τ_g, can then be obtained as well

$$\tau_g = (1 - \Gamma^2)\, e^{-jks}\, e^{-\alpha s}/\Delta \qquad (8.2.2)$$

where:

$k = 2\pi\sqrt{\varepsilon_r}/\lambda$ is the propagation constant inside the slab;

$\alpha = \omega \tan(\delta) \sqrt{\mu_0 \varepsilon_r \varepsilon_0}/2$ is the attenuation coefficient, also inside the slab;

$k_0 = 2\pi/\lambda$ is the free space propagation constant,

and the denominator, $\Delta = 1 - \Gamma^2 e^{-j2ks}\, e^{-2\alpha s}\, e^{jk_0 d \cos(\psi)}$.

The path length inside the slab between the two surfaces is:

propagation for the transmission case; received power from reflection on a perfectly conducting plane for the reflection case.

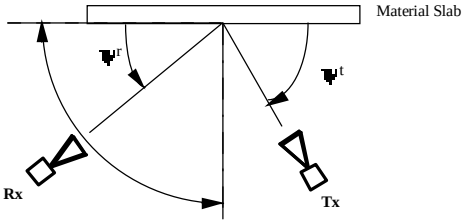

(a) scattering pattern: for several ψ_t, ψ_r varies over range

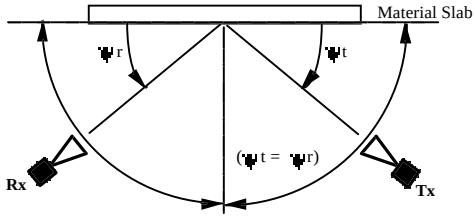

(b) bistatic reflection: $\psi_t = \psi_r$ over range

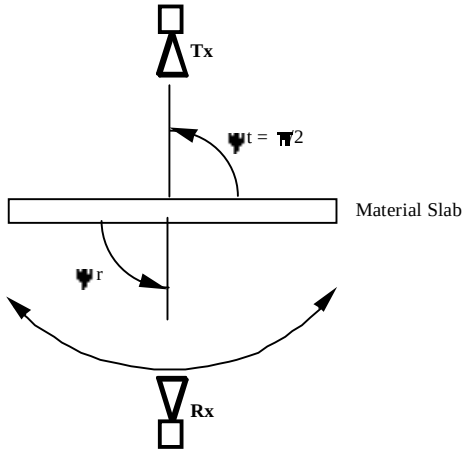

(c) transmission pattern: ψ_t fixed, ψ_r varies over range

Fig. 8.2.1 Measurement setups for power measurements

exclusively on short range propagation effects at mmw. Sections 8.5 and 8.6 contain material which is also relevant to 5.2 and 17.2 GHz operation.

8.2 Material Characterisation

Luis Correia, IST, Portugal

Propagation phenomena at the mmw band can be modeled simply on the basis of Geometrical Optics (GO) since diffraction is usually negligible. The use of GO models requires knowledge of the reflection coefficients of the surfaces, which depend on the electrical properties of the materials. Thus, besides the characterization of the surface roughness, it is essential to know the values of the relative dielectric constant, ε_r, and the loss tangent, $\tan(\delta)$ of the building materials used in both indoor and outdoor environments. The lack of values for these parameters in the literature, in particular at mmw, has motivated the work on materials characterization.

Additionally, the isolation and transmission properties of materials have been calculated, in order to evaluate both indoor coverage in different rooms and co-channel interference not only between indoor and outdoor systems but also among indoor systems.

8.2.1 Measurement Methods

The electromagnetic characteristics, such as ε_r and $\tan(\delta)$, of materials cannot be measured directly in most cases. This implies that other quantities must be measured, from which these parameters can be estimated. The two usual procedures are: 1) to insert a sample of material within a waveguide and perform standing wave measurements, and 2) to illuminate a slab of material in an anechoic chamber, and perform reflected and transmitted power measurements. The first is very difficult to use at the mmw frequencies, since waveguides have dimensions of a few mm and this would imply samples of bricks or plaster, for example, with such dimensions, which is impractical. Therefore, all the measurements were done using the second procedure.

In general, three types of measurements have been conducted, as shown in Fig. 8.2.1(a), (b), and (c). The scattering patterns (a) allow the surface roughness to be investigated. The bistatic reflection (b) corresponds to the measurement of the specular reflection coefficient, from which the parameters can be estimated. The transmission pattern (c) includes the measurement of the actual transmission coefficient, also enabling the estimation of parameters. Measures of reflectivity, R, and transmissivity, T, are special cases. The first corresponds to the bistatic reflection with $\psi_t = \psi_r = \pi/2$ and the second is the transmission with $\psi_t = \pi/2$. In all cases, power is measured relative to a reference: received power from free space

transmitters imposed by safety considerations eliminate the possibility to use IR for reliable broadband communications in cells with radii in excess of about a few metres. A detailed analysis of these considerations is given in reference [1].

8.1.2 Millimetre wave Safety and Technology

Mmw radiation is relatively harmless compared with the conventional mobile UHF frequency bands. The reason is the much smaller electromagnetic skin depth of biological tissues at these frequencies. This is reflected in the existing safety limits of transmitted power. For many European countries, these limits are laid down in the Recommendations of the International Non-Ionizing Committee, a working group of the International Radiation Protection Association (IRPA/INIRC).

The maximum power density for continuous exposure for the general public is 1 mW/cm^2 for mmw. Assuming that this limit is set at 6 cm from an antenna with 9 dBi directivity, the transmitted power is limited to about 50 mW. Limiting transmit power levels to some tens of mW is not only a safety requirement, but also a measure to limit the coverage range in order to improve the frequency reuse capabilities, with the objective of gaining network capacity.

The safety limit of 50 mW transmitted power is about equal to the power level that is feasible with state-of-the-art technology at 60 GHz. A preliminary feasibility study [2] showed that 50 mW might be sufficient for reliable broadband communication in a typical office environment. This may be realizable by taking advantage of advances in Microwave and Millimetre wave Monolithic ICs (M^3ICs), which will supply the signals to the Very High Speed Integrated Circuit (VHSIC) chips at a rate that is compatible with the high processing speeds. The maturity of these technologies has already been demonstrated, although the initial costs of producing such systems can be quite high. However, with large-volume manufacturing of individual circuit functions, the costs can be competitive when compared with installing new copper or fibre networks.

Low-power transmission at mmw frequencies enables improved portability of hand-held equipment because low power implies light and small-sized batteries and mmw radio-frequency components and antennas are small, with dimensions in the order of only a few centimetres. However, it is important to realize that radio receivers for high bit rate signals have to perform complex signal processing order to combat radio channel imperfections to meet the performance requirements. These requirements are much more stringent than requirements for low speed data and coded speech as supported by the present radio networks. Although the intensive signal processing may be performed by sophisticated VHSIC technology it may be expected that the required complexity will contribute significantly to the size and weight of initial broadband radio equipment.

In view of the safety limitations of IR and the apparent lack of suitable blocks of free spectrum below the mmw bands, the next three sections will concentrate

remote from the central base station. This leads to the requirement to support distributed architecture ad-hoc networks.

The chapter is organised as follows: in section 8.1.1 the reasons for rejecting IR are briefly reviewed. Section 8.1.2 covers safety and technology aspects of mmw, leading to the decision to concentrate on these bands. Sections 8.2, 8.3 and 8.4 deal with various aspects of radio propagation at 60 GHz. 8.2 covers the characterisation of building materials in terms of their reflection and scattering properties, and methods of estimating these from measurements of dielectric constant and loss tangent on samples of brick, concrete, plaster, wood, glass, etc. 8.3 deals with narrow-band and wide-band measurements of the indoor radio channel, and compares these with statistical and deterministic models derived from the material properties. 8.4 makes the corresponding comparisons for the outdoor radio channel. Section 8.5 deals with the performance of digital modulation systems over the point-to-point radio channels characterised in the last two sections. Section 8.6 deals with network architectures, both centralised and distributed, and Medium Access Control (MAC) protocols designed to provide efficient and fair sharing of the radio channel among users. Finally, section 8.7 summarises the chapter.

8.1.1 Infra-Red Safety

IR has an abundance of bandwidth free from regulation, and IR components are small and inexpensive. It is already used at very low data rates, eg TV remote control, car keys etc, and at rates up to a few hundred kbit/s for linking palmtop computers. IR penetrates glass, but not walls, allowing neighbouring cells to co-exist without interference. However, the received power levels required by IR systems are much higher than those of radio systems. This is because the photodetector is exposed to ambient noise sources such as sunlight, incandescent and fluorescent lamps, and heaters. An optical filter has been proposed to minimise this effect, but this then becomes a key cost driver. In order to provide full mobility, diffuse links relying on scattering from the local environment are essential, and this leads to transmit power requirements that are beyond the current state of the art.

It is possible to support a 50 Mbit/s transmission rate over distances up to 30 m provided a lens is used to direct the transmited beam towards the intended receiver. However, stringent limitations on power densities a few cm from the transmitter are imposed by eye safety considerations. The human eye focuses the incident light on to the retina increasing the energy density by factors of 100,000 or more. The Maximum Possible Exposure (MPE) levels are therefore quite small. The cornea, the outer layer of the eye, filters out all wavelengths except those in the visible and near infrared range. The eye thus forms a window for infrared light. Exposure to high levels of IR radiation may damage the eye leading to cataract-like disorders. Various standards organizations worldwide have specified MPEs for IR. They are nearly in consensus on a 1.6 mW/cm^2 limit. The power limits on infrared

8

Broadband Systems

Stephen Barton, University of Leeds, UK

8.1 Introduction

This chapter is concerned with wireless communication to mobile, or at least portable, equipment at very high data rates, defined for this purpose as greater than 2 Mbit/s, so as to ensure that there is no overlap with UMTS. Such systems are generally referred to as Wireless Local Area Networks (WLANs). Such fourth generation systems have been addressed by a small group within COST231 (Working Group 3, Broadband Systems) between 1989 and 1996. Such systems will form an increasingly important focus of the proposed follow-on project. Systems operating at data rates up to 155 Mbit/s have been proposed and studied by simulation.

Initially, operating frequencies in the Millimetre Wave (mmw) bands or at Infra Red (IR) were considered the only viable ranges offering sufficiently large contiguous blocks of spectrum not already allocated to other services. IR was eliminated quite early because of considerations of eye safety, and most of the propagation work concentrated on the mmw bands. Subsequently however, spectrum at 5.2 and 17.2 GHz has been allocated by CEPT to HIPERLAN, a system with a transmission rate of 23.5 Mbit/s, and material about broadband transmission in HIPERLAN is included in the later sections.

Material originating in RACE project 2067, Mobile Broadband System (MBS), and ESPRIT project 7359, Local Area network User Radio Access (LAURA), together with many independently funded projects contributing to COST 231 WG3 is also included.

Initial applications of WLANs will be in wired LAN replacement. This is because in large organisations typically 30% of computer networks are relocated or reorganised every year, and this can account for over 80% of the lifetime cost of a LAN. A system providing the last 50 m connection from the end user to the backbone fibre optic network over the air would save most of this. WLANs can also be installed rapidly, often by the users themselves, and may also provide an opportunity to try out the services available before committing to the investment in a full-scale fibre-based network. Access to the services provided by private wired computer networks such as Ethernet and FDDI, or the future ATM based B-ISDN public network will be via centrally controlled access points at data rates high enough to maintain the quality of service. Once such radios are installed in portable equipment, however, there will be a desire to operate in other locations